Tectonophysics 786 (2020) 228450

Contents lists available at ScienceDirect

Tectonophysics

journal homepage: www.elsevier.com/locate/tecto

Crustal seismicity in the Andean Precordillera of Argentina using seismic broadband data

Agostina Venerdini[a,b,*], Patricia Alvarado[a,b], Jean-Baptiste Ammirati[a,1], Marcos Podesta[a], Luciana López[c], Facundo Fuentes[d], Lepolt Linkimer[e], Susan Beck[f]

[a] Grupo de Sismotectónica, Centro de Investigaciones de la Geósfera y la Biósfera (Consejo Nacional de Investigaciones Científicas y Técnicas CONICET– Facultad de Ciencias Exactas, Físicas y Naturales, UNSJ), San Juan, Argentina

[b] Departamento de Geofísica y Astronomía, Facultad de Ciencias Exactas, Físicas y Naturales, Universidad Nacional de San Juan, San Juan, Argentina

[c] Instituto Nacional de Prevención Símica, San Juan, Argentina

[d] YPF S.A., Buenos Aires, Argentina

[e] Escuela Centroamericana de Geología, Universidad de Costa Rica, San José, Costa Rica

[f] Department of Geosciences, University of Arizona, Tucson, AZ, United States

ARTICLE INFO

Keywords:
Crust
Focal mechanism
Fold-thrust belt
Andean retroarc
Flat slab
South America

ABSTRACT

In this study, we analyze 100 crustal Precordilleran earthquakes recorded in 2008 and 2009 by 52 broadband seismic stations from the SIEMBRA and ESP, two temporary experiments deployed in the Pampean flat slab region, between the Andean Cordillera and the Sierras Pampeanas in the Argentine Andean backarc region.

In order to determine more accurate hypocenters, focal mechanisms and regional stress orientations, we relocated 100 earthquakes using the JHD technique and a local velocity model. The focal depths of our relocated events vary between 6 and 50 km. We estimated local magnitudes between $0.4 \leq M_L \leq 5.3$ and moment magnitudes between $1.3 \leq M_w \leq 5.3$. Focal mechanisms were determined from new hypocenter relocations and first motion P-wave polarities. Our solutions exhibit a majority of the earthquakes with reverse faulting mechanism. Regional stress tensor from the inversion of P- and T-axis orientations, shows a maximum stress axis (σ_1) almost horizontal with a strike of 85° and a minimum stress axis (σ_3) almost vertical.

We correlate this small-to-moderate magnitude seismicity with the presence of large basement structures beneath the Iglesia-Calingasta Basin in the west and the Eastern Precordillera in the east. The nucleation of deep earthquakes beneath the Iglesia Basin could be related to the presence of a major ramp accommodating the crustal shortening between the Frontal Cordillera and the Precordillera. The crustal seismicity beneath the Precordillera seems to correlate with west-dipping structures rooting deep into the Cuyania basement suggesting a thick-skinned basement deformation system beneath the Precordillera and its shallow thin-skinned fold and thrust belt.

1. Introduction

The Precordillera region is located in the South American continental plate above the horizontal subduction of the Nazca plate and to the east of the Main and Frontal Cordilleras, where active volcanism ceased since the last 15.2–6.3 My (Fig. 1) (Kay and Abbruzzi, 1996; Ramos and Folguera, 2009). The style of upper crustal deformation of the Precordillera is described as a thin-skinned fold-thrust belt (Rolleri, 1969; Ramos, 1988; Allmendinger et al., 1990; Cristallini and Ramos, 2000). Comparatively, many more earthquakes have been reported in the thick-skinned Sierras Pampeanas region located several hundred kilometers east of the Precordillera (Fig. 2) (Alvarado et al., 2005; Monsalvo et al., 2014; Richardson et al., 2012).

Over the past decades, the flat-slab segment of the Argentine Andean retroarc has been the focus of numerous studies (e.g. Barazangi and Isacks, 1976; Cahill and Isacks, 1992; Reta, 1992; Pardo et al., 2002, 2004; Anderson et al., 2007; Alvarado et al., 2009a, 2009b; Gans et al., 2011), although crustal seismicity in the Precordillera has not been studied in detail except for early contributions from Smalley and Isacks (1990), Smalley et al. (1993) and Pujol et al. (1991). Possible

* Corresponding author at: Av. Ignacio de la Roza 590, Complejo Universitario "Islas Malvinas", FCEFN, Universidad de San Juan, CP: J5402DCS Rivadavia, San Juan, Argentina.

E-mail address: agostina.venerdini@unsj-cuim.edu.ar (A. Venerdini).

[1] Now at: Agencia Nacional de Investigación y Desarollo (ANID-FONDECYT N°3200633), Departamento de Geología, Universidad de Chile, Santiago, Chile.

https://doi.org/10.1016/j.tecto.2020.228450
Received 20 October 2019; Received in revised form 14 March 2020; Accepted 10 April 2020
Available online 03 May 2020
0040-1951/

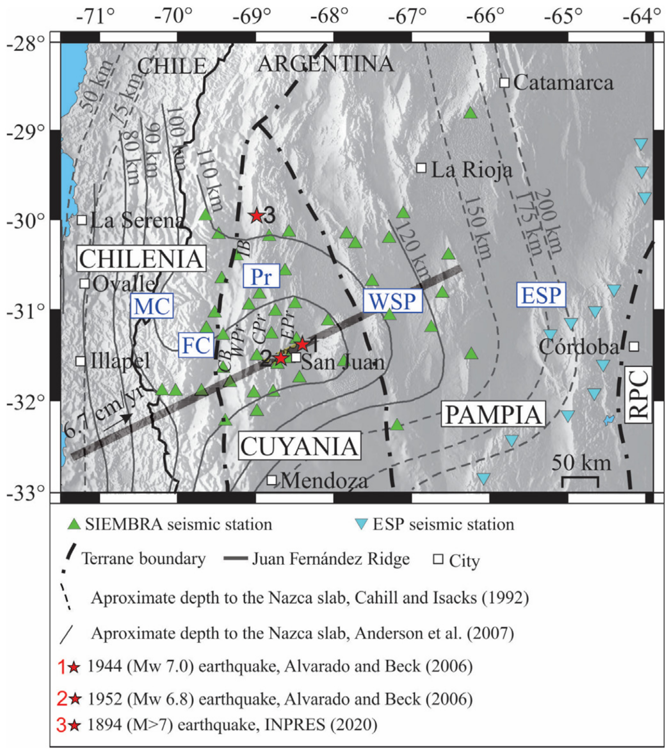

Fig. 1. Regional map around the flat slab region of the South Central Andes showing the locations of the SIEMBRA and ESP broadband IRIS-PASSCAL deployments, respectively and main cities. Depths to the slab contours and epicenters of the large Andean Precordilleran damaging crustal earthquakes (Alvarado and Beck, 2006; Rivas et al., 2019) are shown. The thick gray line shows the approximate path of the Juan Fernández Ridge. The convergence rate between the Nazca and South American plates from GNSS observations is represented by the black arrow (Vigny et al., 2009). Terranes and main morphostructural units are MC: Main Cordillera, FC: Frontal Cordillera, Pr: Precordillera, WSP: Western Sierras Pampeanas, ESP: Eastern Sierras Pampeanas according to Ramos et al. (2002), RPC: Rio de la Plata Craton, WPr: Western Precordillera, CPr: Central Precordillera, EPr: Eastern Precordillera, IB: Iglesia Basin and CB: Calingasta Basin according to Baldis and Chebli (1969), Ortiz and Zambrano (1981), Baldis and Bordonaro (1984), Ramos (1988) and Rapela (2000).

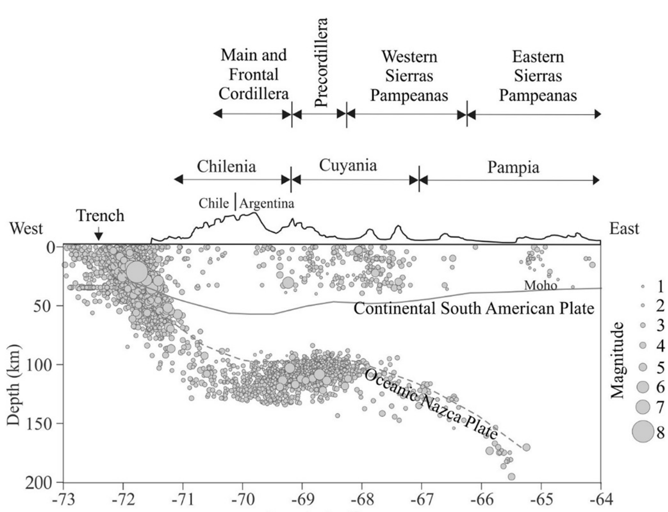

Fig. 2. East-west cross section showing seismicity during 17 years (2000–2017) from ISC (2020) in the western margin of South America at ~31°S. Magnitudes are between $1.3 \leq M_w \leq 8.3$. The main morphostructural units and terranes are the same as described in Fig. 1.

reasons for this are the relatively scarce occurrence of moderate to large sized crustal seismicity during modern times and the lack of good quality pre-digital world-wide instrumental recordings. Alvarado and Beck (2006) and Meigs and Nabelek (2010) used teleseismic data to study the Eastern Precordillera historical earthquakes of 1944 (M_w 7.0) and 1952 (M_w 6.8), which have caused deaths and severe damage to the city of San Juan in western Argentina (Fig. 1, Table 1). Another problem is the uncertain detection of smaller magnitude seismicity by permanent seismic stations at regional distances. This seismicity is more abundant but the scarce coverage of it is not good enough for accurate automatic source characterization, especially in the Precordillera area (Sánchez et al., 2013). A noticeably higher seismic activity can be observed for the Andean backarc at intermediate depths between 100 km and 120 km, in the horizontal segment of the Nazca subducting plate (Fig. 2). In contrast, very little seismicity is detected in the upper continental plate at shallow depths < 50 km in the Precordillera.

In this study, we perform the relocation of 100 crustal events recorded between 2008 and 2009 in the Precordillera by temporary seismic deployments, using the Joint-Hypocenter-Determination (JHD) method (Pavlis and Booker, 1983; Pujol, 1988) and compare our relocation results with previous hypocenter solutions presented in Val et al. (2018). We also calculate and compare local and moment magnitude estimations (M_L and M_w, respectively). Finally, we calculate new focal mechanisms from the relocated seismicity using an increased number of P-wave first motions and determine an average estimation of the main stress axis orientations.

We analyze our results in the framework of historical large earthquakes that have occurred in the area as well as the crustal seismicity determinations and tectonic interpretations from the PANDA (Portable Array for Numerical Data Acquisition; Chiu et al., 1991) experiment for two small sectors in the Precordillera (Smalley et al., 1993). This helps to characterize seismic and non-seismic zones within the Precordillera (including the Central and Western Precordillera, more to the west, where PANDA had no coverage) at different depths in the crust. This information is key to understand the depth at which the current deformation of the Precordillera occurs as well as the tectonic features responsible for such deformation.

1.1. Seismic experiments and crustal thickness estimations in the Precordillera

This study focuses on crustal earthquake characterization beneath the Andean Precordillera. We use approximately two years of continuous three-components broadband seismological records from the SIEMBRA (***SI****erras* ***E****xperiment using a* ***M****ulticomponent* ***BR****oadband* ***A****rray*; Beck and Zandt, 2007) and the ESP (***E****astern* ***S****ierras* ***P****ampeanas;* Gilbert, 2008) IRIS-PASSCAL experiments. The SIEMBRA network consisted of the deployment of 40 stations during 2008 and 2009 in the Main and Frontal Cordilleras, Precordillera and Western Sierras Pampeanas. Simultaneously, 12 broadband seismic stations were deployed as part of the ESP network, along the Eastern Sierras Pampeanas (Fig. 1).

Regnier et al. (1994), Gilbert et al. (2006), Gans et al. (2011) and Ammirati et al. (2015) show that the crustal thickness for the Precordillera varies between 66 km in the west, to 55 km in its eastern region. Ammirati et al. (2015) and Ammirati et al. (2018) also constrained a lithospheric scale S-wave velocity using the joint inversion of receiver functions and Rayleigh wave phase velocity dispersion. The seismic velocity model by Ammirati et al. (2015) shows the presence of several upper-plate middle-crustal discontinuities, zones of high S-wave velocity in the upper-plate lower crust associated with a weak Moho signal consistent with the hypothesis of partial eclogitization in the lower crust and the presence of low S-wave velocities at ~100 km depth interpreted as hydrated basaltic oceanic crust.

We compare the earthquakes in this study with the seismicity reported in the global ISC (2020) catalog from 2000 to 2017, for a cross-

Table 1
Relocated hypocenters and seismic source parameters obtained using the Joint-Hypocenter-Determination JHD program (Kissling et al., 1994). Seismic relocation parameters include origin time (year, month, day, UTC hour, minute, second), epicenter (latitude, longitude), focal depth, root mean square (RMS), GAP of back azimuths; local magnitude (M_L) and moment magnitude (M_w, Val et al., 2018) are also reported. Last columns show focal mechanisms with indication of the two potential fault-plane solutions as a combination of strike, dip and rake (Aki and Richards (1980)'s convention is assumed). Theses relocated results are shown in Figs. 5, 6, and 10. Events shown with * and ** correspond to SIEMBRA events determined using waveform modeling by Alvarado et al. (2010) and Ammirati et al. (2015), respectively. Events with *** correspond to the historical earthquakes that occurred in the Precordillera (Alvarado and Beck, 2006). Event shown with **** is from INPRES (2020).

Event	Year	Month	Day	Hour	Minute	Second	Latitude (°)	Longitude (°)	Depth (km)	RMS (s)	GAP (°)	M_L	M_w	Nodal plane 1			Nodal plane 2		
														Strike (°)	Dip (°)	Rake (°)	Strike (°)	Dip (°)	Rake (°)
1	2008	1	23	8	53	3.7	−30.133	−69.393	30.51	0.29	119	3.5	3.7	12	43	90	192	47	90
2	2008	1	28	6	38	51.7	−31.792	−68.874	24.23	0.27	54	2	2.5	91	77	54	344	38	159
3	2008	1	28	9	40	35.7	−31.792	−68.874	24.18	0.3	54	2.7	3	138	41	90	318	49	90
4	2008	1	30	17	13	11.2	−30.251	−68.868	32.48	0.65	96	2.3	2.8	213	82	70	102	21	158
5	2008	2	18	20	3	57.2	−30.847	−68.357	24.7	0.26	64	2.5	2.8	232	18	40	103	79	104
6	2008	2	25	23	55	1.4	−31.741	−69.515	49.45	0.34	94	3	3.2	9	12	90	189	78	90
7	2008	3	13	20	0	54.2	−30.714	−68.386	38.62	0.18	76	1.8	2.4	113	30	−81	283	60	−95
8	2008	3	28	18	0	28.7	−30.291	−68.9	33.73	0.3	113	2.1	2.6	244	69	−88	58	21	−95
9	2008	4	7	8	42	34.8	−31.897	−69.447	38.57	0.42	100	2.8	3	4	40	82	194	50	97
10	2008	4	7	15	24	8.2	−30.576	−68.478	34.6	0.23	63	1.9	2.5	336	65	7	243	84	155
11	2008	4	11	12	13	9.2	−30.229	−68.431	28.43	0.26	130	2.4	2.8	293	32	−87	109	58	−92
12	2008	4	13	22	52	33.9	−31.236	−68.781	40.63	0.18	28	2.1	2.6	174	45	40	53	63	127
13	2008	4	16	13	58	9.5	−30.247	−69.399	29.12	0.47	119	2.4	2.8	180	76	51	73	41	158
14	2008	4	25	4	25	12.2	−30.633	−68.496	35.85	0.18	57	1.9	2.4	81	22	−52	221	73	−104
15	2008	4	25	4	31	4	−31.602	−68.746	27.34	0.35	66	3.2	3.4	358	42	87	182	48	93
15*	2008	4	25	4	31	0	−31.599	−68.743	30	–	–	–	3.5	220	54	82	53	37	101
16	2008	5	15	5	18	36.5	−31.546	−68.857	21.97	0.22	49	2.3	2.7	263	71	79	114	22	119
17	2008	5	15	14	47	0.2	−31.324	−68.566	25.1	0.61	37	1.9	2.4	21	71	75	240	24	127
18	2008	5	23	22	45	59	−31.888	−68.644	26.46	0.22	125	3	3.2	323	43	17	220	78	132
19	2008	5	29	3	22	28.4	−31.161	−68.191	41.64	0.21	54	1.9	2.4	320	73	70	191	26	138
20	2008	6	12	21	40	22.1	−30.595	−68.304	44.41	0.24	70	1.7	2.3	302	38	14	201	81	127
21	2008	6	16	3	59	23.6	−31.804	−68.799	18.11	0.34	60	1.7	2.2	196	79	−68	311	24	−153
22	2008	6	22	22	12	37.8	−30.453	−69.442	35.15	0.24	136	1.9	2.5	335	70	89	158	20	93
23	2008	7	1	1	19	25.8	−31.667	−68.798	23.37	0.2	62	2.7	3	255	74	89	79	16	93
24	2008	7	11	19	42	59.3	−31.695	−68.6	27.65	0.34	101	2.1	2.6	215	60	88	39	30	93
25	2008	7	22	2	35	4.6	−30.445	−69.321	24.72	0.31	123	2	2.5	352	46	−76	152	46	−104
26	2008	8	2	0	30	44.9	−31.217	−68.517	39.56	0.14	30	1.6	2.2	26	46	90	206	44	90
27	2008	8	3	0	16	17.4	−30.637	−68.413	32.23	0.19	61	2.3	2.7	119	34	−32	236	73	−120
28	2008	8	3	18	10	10.1	−30.36	−69.424	32.88	0.23	131	2.4	2.7	160	81	61	54	30	162
29	2008	8	5	6	38	13.5	−30.336	−69.319	32.04	0.23	116	2.5	2.9	5	45	90	185	45	90
30	2008	8	6	15	8	48.4	−31.465	−68.637	25.33	0.23	48	1.9	2.4	1	43	90	181	47	90
31	2008	8	18	11	56	39.7	−31.962	−68.858	22.16	0.24	113	1.8	2.4	0	44	90	180	46	90
32	2008	8	24	2	27	27.2	−31.363	−68.825	36.76	0.2	33	2.4	2.7	345	32	59	200	63	108
33	2008	9	5	2	21	14.3	−30.616	−69.4	23.14	0.41	127	2.4	2.8	87	46	76	287	46	104
34	2008	9	10	14	15	10.4	−30.689	−69.016	30.47	0.28	53	2	2.5	244	48	−62	26	49	−118
35	2008	9	16	23	59	5.9	−30.377	−69.372	40.39	0.3	126	1.9	2.4	172	71	−81	326	21	−114
36	2008	9	20	12	47	1.6	−31.096	−68.558	36.74	0.22	28	1.9	2.4	77	8	−82	249	82	−91
37	2008	9	21	17	14	50.7	−31.18	−68.501	38.18	0.3	37	2.2	2.6	20	36	83	209	54	95
38	2008	9	25	11	34	33.2	−30.351	−69.39	33.91	0.22	127	2	2.5	189	35	88	11	55	91
39	2008	9	27	8	4	18	−31.725	−68.736	19.64	0.3	75	3.7	3.8	356	51	65	213	45	118
39*	2008	9	27	8	4	18	−31.715	−68.719	21	–	–	–	4	66	51	82	259	40	100
40	2008	9	30	6	51	11.7	−31.121	−68.291	31.67	0.17	51	1.7	2.4	167	63	89	349	27	92
41	2008	9	30	10	10	38.9	−31.269	−68.383	39.1	0.19	62	1.4	2.1	57	30	90	237	60	90
42	2008	10	4	22	20	10.4	−31.424	−68.703	32.48	0.96	41	1.8	2.3	75	22	−68	231	70	−99
43	2008	10	9	7	43	32.4	−31.504	−68.703	27.36	0.23	52	2	2.5	169	44	90	349	46	90
44	2008	10	13	2	3	11.1	−31.093	−68.507	38.94	0.51	37	1.7	2.3	90	77	35	351	56	164
45	2008	10	14	17	10	49.1	−31.168	−68.188	42.45	0.25	55	1.9	2.5	16	20	81	206	70	93
46	2008	10	24	4	46	22.5	−30.128	−69.002	32.77	0.37	150	2.2	2.7	179	46	66	32	49	113

(continued on next page)

Table 1 (*continued*)

Event	Year	Month	Day	Hour	Minute	Second	Latitude (°)	Longitude (°)	Depth (km)	RMS (s)	GAP (°)	M_L	M_w	Nodal plane 1			Nodal plane 2		
														Strike (°)	Dip (°)	Rake (°)	Strike (°)	Dip (°)	Rake (°)
47	2008	11	7	11	26	24	−31.57	−69.417	8.28	0.49	89	3.8	4.1	308	39	−30	62	72	−125
47**	2008	11	7	11	26	–	−31.652	−69.347	2	–	–	–	3.8	18	51	113	164	44	64
48	2008	11	8	20	54	44.5	−30.481	−69.331	24.72	0.58	125	2.4	2.8	175	51	90	355	39	90
49	2008	11	9	5	2	31.1	−31.58	−69.431	5.89	0.57	91	1.6	2	319	81	−89	133	9	−96
50	2008	11	11	5	27	36.8	−30.711	−68.375	30.63	0.45	56	1.8	2.4	182	70	89	5	20	93
51	2008	11	12	19	37	28.9	−31.186	−68.592	36.3	0.19	27	1.7	2.3	348	83	57	247	34	167
52	2008	11	21	16	13	1.7	−31.408	−68.604	23.61	0.23	40	2	2.5	131	30	20	24	80	118
53	2008	11	27	19	41	2.9	−31.178	−68.36	37.78	0.22	54	1.7	2.3	118	72	−74	255	24	−130
54	2008	12	3	20	35	22.4	−31.311	−69.443	25.44	0.35	76	2.1	2.6	0	75	90	180	15	90
55	2008	12	6	4	23	44.7	−31.182	−69.472	25.1	0.27	83	2.4	2.8	296	67	−87	108	23	−97
56	2008	12	9	12	4	2.9	−30.612	−69.405	23.74	0.4	133	2	2.5	172	32	−60	318	63	−107
57	2008	12	10	5	42	17.7	−31.446	−68.742	25.97	0.18	34	1.8	2.4	100	60	−56	227	44	−134
58	2008	12	14	21	41	58	−31.215	−68.298	36.31	0.19	55	1.6	2.2	350	20	40	222	77	106
59	2008	12	17	7	26	32.4	−29.891	−68.593	21.19	0.28	173	1.6	2.2	0	24	90	180	66	90
60	2008	12	26	9	5	48.6	−30.187	−68.857	32	0.51	151	2.3	2.7	159	79	49	57	42	163
61	2009	1	11	5	27	8.7	−31.594	−69.422	10.89	0.57	90	4.1	4.5	338	51	64	196	46	118
61*	2009	1	11	5	27	0	−31.66	−69.27	5	–	–	–	4.2	169	49	75	11	43	107
61**	2009	1	11	5	27	–	−31.557	−69.269	1	–	–	–	4	165	36	64	17	58	108
62	2009	1	12	11	8	19.4	−31.342	−68.808	36.65	0.23	31	1.9	2.5	339	20	−31	98	80	−107
63	2009	1	13	8	35	15.7	−30.563	−69.33	28.61	0.26	112	2.1	2.6	38	20	−55	181	74	−102
64	2009	1	18	35	6	5.4	−31.07	−68.449	31.29	0.27	45	1.8	2.4	0	32	90	180	58	90
65	2009	1	18	14	54	0.8	−30.325	−69.495	38.84	0.42	140	2.8	3.1	13	37	−62	159	58	−109
66	2009	2	10	2	58	34.2	−31.417	−68.787	30	0.15	36	1.6	2.2	348	23	12	247	85	113
67	2009	2	10	4	49	0	−30.355	−69.428	35.69	0.31	132	1.9	2.4	48	20	−55	191	74	−102
68	2009	2	10	19	23	27.9	−30.073	−68.749	26.59	0.31	158	2.5	2.9	12	51	46	249	56	131
69	2009	2	16	21	55	45.1	−30.646	−69.006	30.67	0.46	56	1.7	2.2	124	55	72	334	39	114
70	2009	3	8	12	43	1.1	−31.67	−69.363	23.11	0.27	50	2.8	3.1	140	59	88	324	31	93
71	2009	3	11	12	53	38.5	−31.948	−69.393	25	0.41	97	2.1	2.6	11	49	90	191	41	90
72	2009	3	11	13	6	50.4	−31.962	−69.4	28.88	0.36	99	5.3	5.3	326	55	50	202	51	133
72*	2009	3	11	13	6	51	−31.89	−69.19	29	–	–	–	5.3	317	36	75	156	55	101
72**	2009	3	11	13	6	–	−31.98	−69.29	28	–	–	–	5.2	339	42	75	179	50	103
73	2009	3	11	13	21	0.9	−31.955	−69.397	26.55	0.34	98	2.8	3.1	131	65	90	311	25	90
74	2009	3	20	4	16	41.5	−31.183	−68.536	38.63	0.15	27	2	2.4	196	40	81	28	51	97
75	2009	3	22	8	7	6.2	−31.899	−69.137	17.69	0.33	65	1.9	2.3	148	3	90	328	87	90
76	2009	3	22	9	56	59.5	−30.963	−68.54	21.18	0.29	54	1.8	2.3	23	64	90	203	26	90
77	2009	4	9	20	29	59	−31.446	−69.314	34.95	0.31	72	2.2	2.7	329	62	25	227	68	150
78	2009	4	10	7	57	53.4	−31.467	−68.678	19.88	0.35	48	1.6	2.2	224	37	85	50	53	94
79	2009	5	10	22	17	8.9	−31.325	−68.691	29.39	0.14	36	2.2	2.6	347	47	52	216	55	123
80	2009	5	10	22	22	9	−30.936	−68.709	26.57	0.25	33	1.9	2.4	233	41	−83	44	49	−96
81	2009	5	16	10	45	15.6	−30.298	−68.597	50.01	0.25	116	3.8	3.8	322	56	44	204	55	137
82	2009	5	22	7	14	40	−31.483	−68.687	26.91	0.31	50	2.1	2.5	7	41	72	210	51	105
83	2009	6	5	6	41	4.3	−31.438	−68.792	26.78	0.22	39	1.8	2.4	41	68	−88	216	22	−95
84	2009	6	7	9	3	54.1	−31.173	−68.592	39.2	0.21	34	1.7	2.2	299	31	−89	118	59	−91
85	2009	7	18	21	3	3.3	−30.581	−69.01	39.99	0.23	63	2.1	2.6	226	65	−86	37	25	−99
86	2009	8	20	8	10	30.5	−30.804	−69.085	17.88	0.24	78	0.4	1.3	2	70	90	182	20	90
87	2009	9	19	6	50	32.3	−30.419	−69.435	30.62	0.21	147	2.9	3.2	154	76	−88	326	14	−98
88	2009	9	23	18	9	7.5	−31.324	−68.687	29.08	0.16	34	2	2.5	194	33	88	16	57	91
89	2009	9	29	1	40	55.2	−31.672	−68.691	27.32	0.16	116	0.4	1.6	0	38	90	180	52	90
90	2009	10	5	10	31	26.5	−31.183	−68.658	38.75	0.15	29	1.7	2.4	0	46	90	180	44	90
91	2009	10	12	3	22	31.4	−30.887	−68.698	23.6	0.28	34	2.3	2.8	36	16	−51	176	78	−100
92	2009	10	13	18	50	7	−31.14	−68.2	42.41	0.18	52	1.8	2.3	0	27	90	180	63	90
93	2009	10	25	5	48	55.2	−31.343	−69.42	24.07	0.33	105	2.5	2.8	273	48	89	94	42	91
94	2009	11	1	15	4	54.4	−31.934	−69	23.32	0.29	73	1.8	2.4	309	65	−89	127	25	−92

(*continued on next page*)

Table 1 (*continued*)

Event	Year	Month	Day	Hour	Minute	Second	Latitude (°)	Longitude (°)	Depth (km)	RMS (s)	GAP (°)	M_L	M_w	Nodal plane 1			Nodal plane 2		
														Strike (°)	Dip (°)	Rake (°)	Strike (°)	Dip (°)	Rake (°)
95	2009	11	4	2	31	31.1	−31.377	−68.849	35.14	0.11	57	0.4	1.6	2	59	90	182	31	90
96	2009	11	4	6	18	34.9	−31.385	−68.523	34.52	0.18	41	1.7	2.2	224	31	88	46	59	91
97	2009	11	7	12	9	21.8	−30.164	−69.01	28.34	0.27	129	2.3	2.8	347	60	−88	163	30	−93
98	2009	11	15	11	45	18.2	−31.579	−68.664	34.15	0.24	66	2.1	2.6	331	23	12	230	85	113
99	2009	11	15	14	32	13.2	−31.309	−68.937	37.38	0.25	43	1.5	2.1	1	55	75	206	38	110
100	2009	11	17	6	2	45.4	−31.352	−68.693	30.81	0.13	35	1.7	2.3	114	82	−83	253	11	−131
***	1944	1	15	23	49	27	−31.40	−68.4	15	–	–	–	7	45	35	110	201	57	76
***	1952	6	11	0	31	37	−31.60	−68.6	12	–	–	–	6.8	40	75	30	301	61	163
****	2010	2	27	6	51	16	−31.68	−68.18	31.2	–	–	–	6 Mb	–	–	–	–	–	–

* Alvarado et al. (2010)
** Ammirati et al. (2015)
*** Alvarado and Beck (2006)
**** INPRES (2020)

section at 31°S (Fig. 2). Our results correspond with the 20% of the earthquakes that occur at crustal depths in the Precordillera while the remaining 80% in this zone corresponds to hypocenters in the flat slab subducted Nazca plate (Fig. 2), in good agreement with previous seismicity studies (Barazangi and Isacks, 1976; Isacks and Barazangi, 1977; Smalley and Isacks, 1987; Smalley and Isacks, 1990; ISC, 2020).

1.2. Previous seismic studies in the Precordillera

Smalley and Isacks (1990) analyzed Argentine National Institute for Seismic Prevention (INPRES) seismic records available for years 1984 to 1985 and observed an increased seismicity concentrated southeast of the Eastern Precordillera around 31.1°S, distributed between 20 km and 30 km depths. They concluded that those depths were unusual for intraplate earthquakes and suggested a brittle/ductile transition at 30–35 km depth. They also suggested that the Western and Central Precordillera seemed aseismic.

Smalley et al. (1993), using data recorded by the PANDA network during 1987 and 1988, initially processed the data using HYPOINVERSE (Klein, 1978) and a laterally homogeneous three-layer crustal velocity model based on suggestions from Bollinger and Langer (1988) and Volponi (1968). They subsequently tested the results using the JHD method. Their seismicity in the Eastern Precordillera, had occurrence in three segments from north to south. The north and central segments show well-defined hypocenter distributions in planes correlating with crustal scale faults that extend from 5 to 35 km depth, while the southern sector shows diffuse seismic activity that does not follow a trend between the Eastern Precordillera and the Western Sierras Pampeanas. In addition, they proposed that this seismicity was the result of the reactivation of ancient structures or were occuring in the basement of unknown affinity west of the suture between terranes.

More recently, Val et al. (2018) presented a discussion about the regional distribution of earthquakes with respect to erosion rates for which they obtained locations for a total of 100 crustal earthquakes (see Table S1). Val et al. (2018) earthquake locations and moment magnitudes M_w were calculated using the Seisan 10.3 software (Ottemöller et al., 2014) and a regional lithospheric velocity model from Ammirati et al. (2015).

Rivas et al. (2019) analyzed 44 small-to-moderate earthquakes more to the north of the present studied region between 28°S and 30.5°S and 68.5°W and 69.5°W. They integrated seismic records of the CHARGE and SIEMBRA temporary seismological stations as well as the INPRES permanent network. They identified P- wave and S-wave first arrivals to locate earthquakes using SEISAN (Ottemöller et al., 2014) and an average seismic velocity model from Sánchez et al. (2013). In addition, they calculated focal mechanisms using P-wave first motions and amplitude ratios between P- and S-waves, seismic moment, coda magnitude, local magnitude and moment magnitude. Their determined seismicity is distributed at upper-to-middle crustal depths (10 to 30 km) with an absence of seismicity at depper levels than 40 km depth in a zone characterized by a crustal thickness of 65 km (Gans et al., 2011; Ammirati et al., 2015). The focal mechanisms are mainly reverse solutions with some slight strike-slip components. Rivas et al. (2019) also proposed a 3D model integrating information from one seismic reflection line, modern seismicity, geological maps, geological cross sections, and outcrop observations, indicating a fractured and seismically active basement between 10 and 30 km depths, just beneath the thin-skinned aseismic top level of the exposed Precordillera.

Linkimer et al. (2020) obtained earthquake locations and a detailed 3D velocity model of the flat slab subduction zone including the Precordillera using regional-scale double difference tomography and the same SIEMBRA-ESP broadband data. They only selected the events detected by > 30 stations and the event set was completed with all reported events from the INPRES and NEIC catalogs. The velocity inversions used 1157 earthquakes with a gap lower than 180°, at least 10 P-wave and 6 S-wave observations, and included at least one observation within a distance of 1.5 times their focal depth. The dataset showed earthquake depths from 0 to 40 km within the crust and from 100 to 200 km within the subducting Nazca plate. They determine Vp, Vs and Vp/Vs for both the South American plate and the Nazca plate and interpret the possible lithologies present in those sectors and the processes that take place there.

2. Geotectonic setting

The Nazca plate between 29°S and 32°S is subducting nearly horizontally beneath the South American plate (Barazangi and Isacks, 1976; Smalley and Isacks, 1987; Cahill and Isacks, 1992; Reta, 1992; Alvarado et al., 2009b; Gans et al., 2011) with a GNSS velocity rate of 6.7 cm/yr and an azimuthal orientation of 74° (Vigny et al., 2009) (Fig. 1). The flattening in the slab subduction, which is well defined by hypocenters locations, at about 100 km depth (Anderson et al., 2007; Linkimer et al., 2020), has been associated with the subduction of the Juan Fernandez Ridge (JFR) (Yáñez et al., 2002). Stuessy et al. (1984) have proposed that the origin of this oceanic mountain range is due to the north-easterly motion of the Nazca plate above the hotspot located at approximately 34°S and 82°W in the Pacific Ocean (Von Huene et al., 1997; Steinberger, 2000).

2.1. Accreted terranes and morphological units

Several accreted terranes characterize the Andean margin in this region of Argentina and Chile (Fig. 2). According to Ramos (1984) and Ramos et al. (1998), the Cuyania terrane and the Chilenia terrane were part of Laurentia and were amalgamated during the Ordovician and Late Devonian to the protomargin of Gondwana (Fig. 1). The contact between Chilenia and Cuyania (Ramos et al., 1986; Davis et al., 2000) is suggested on the base of a belt of mafic-ultramafic rocks and associated metasedimentary rocks that are frequently interpreted as dissected ophiolites (Ramos et al., 2000). The ophiolite belt currently lies in the western margin of the Precordillera (Caminos, 1979) and is associated with the suture between both terranes. The Cuyania terrane comprises the Precordillera and the Western Sierras Pampeanas (Ramos et al., 1998; Ramos, 2004). The basement of Cuyania is composed of Grenville rocks, which have been related to the southern extension of the Appalachian system in the Ouachita embayment (Thomas and Astini, 1996). This basement and its sedimentary cover comprise one of the best studied terranes in this continental margin (Thomas and Astini, 2003; Vujovich et al., 2004). The Chilenia terrane presents high grade metamorphic rocks exposed to the west of the ophiolitic rocks that separate Cuyania from the Chilenia terrane (Ramos et al., 2010). Crustal thickness observations along the Chilenia terrane indicate about 70 km and ~65 km beneath the Western Precordillera (Cuyania) (Regnier et al., 1994; Ammirati et al., 2015). Ammirati et al. (2016) evidenced a difference in crustal thickness as a possible double Moho beneath the Precordillera using stacked local receiver function images. This is related to the presence of a major structure that separates the Cuyania terrane from the more felsic, thicker Chilenia terrane. The region in between the Chilenia and Cuyania terranes can be followed for > 400 km in a north-south orientation and down to ~40 km depth, dipping to the west with probable reverse motion. This major structure may have played an important role in controlling the regional deformation since the Ordovician. Currently, the crustal shortening accommodation may also be occurring in the lower crust, contributing to the complex Moho geometry and the unusually high crustal thickness observed beneath the Chilenia (with a deeper Moho) and Cuyania (with a relatively shallower Moho) terranes. From west to east, this Andean retroarc region comprises the structures of the Main Cordillera and Frontal Cordillera in the Chilenia terrane; Precordillera and Western Sierras Pampeanas in the Cuyania terrane and the Eastern Sierras Pampeanas in the Pampia terrane (Ramos, 1999a) (Fig. 1). The Main Cordillera at this latitude forms a relatively narrow strip of mostly Mesozoic strata deformed by thin-skinned thrust systems (Cristallini and Ramos, 2000). To the east, the Frontal Cordillera is characterized by thick-skinned deformation and relatively low amounts of shortening (Allmendinger et al., 1990; Ramos, 1999b; Heredia et al., 2002). The Frontal Cordillera is separated from the Precordillera by the Iglesia-Calingasta Basins (Fig. 1) (Amos, 1972; Amos and Rolleri, 1965; González, 1985; Allmendinger et al., 1990; Beer et al., 1990; Cortés, 1993; Ramos et al., 2002; Ruskin and Jordan, 2007). The Iglesia-Calingasta Basin corresponds to a regional feature located 250 km east from the subduction trench, and about 100 km above the subducted Nazca plate. The deformation in this region is characterized by reverse motion along N-S trending structures (e.g. Allmendinger and Judge, 2014). The Iglesia-Calingasta Basin contains ~3.5 km deposits (Beer, 1989; Beer et al., 1990) in a region of crustal thickness of about 65 km Ammirati et al. (2015). Thus, the region might have been affected by compression since the Paleozoic involving some periods of extension (Von Gosen, 1992; Alonso et al., 2008), with records of shortening and thickening (Gans et al., 2011; Allmendinger and Judge, 2014); in addition, evidence of transpression during the Neogene has also modified pre-existing structures (Siame et al., 1996; Perucca and Bastías, 2011; Rivas et al., 2019).

2.2. Precordillera, its transition to Sierras Pampeanas and seismic activity

On the basis of the different stratigraphic and structural characteristics, the Precordillera, in general is subdivided into Western, Central and Eastern parts (Fig. 1) (Baldis and Chebli, 1969; Ortiz and Zambrano, 1981; Baldis and Bordonaro, 1984). The Western Precordillera involves mostly Paleozoic, Triassic and Andean foreland basin strata with thin-skinned deformation (e.g. Allmendinger and Judge, 2014) and local inversion of Triassic half-grabens (Barredo and Ramos, 2009). The lower Paleozoic section of this belt is defined by clastic Ordovician deep marine deposits (Spalletti et al., 1989).

The Central Precordillera is characterized by a series of thrust sheets involving Ordovician to Carboniferous strata capped by narrow strips of Neogene foreland basin strata. Unlike the Western Precordillera, the Ordovician section in the Central Precordillera is mostly characterized by carbonate platform strata. Geological observations reflect a style of thin-skinned structures, with large imbricated thrust sheets and local duplex systems (Furque et al., 1999; Ramos and Vujovich, 2000; Anselmi et al., 2006). Both the Western and Central Precordilleras show a dominant eastward vergence.

The Eastern Precordillera has opposite (westward) vergence and is characterized by Cambrian carbonate units that are not observed in thrust systems further west (Ramos and Vujovich, 2000). Unlike the Western and Central Precordillera, deformation along the Eastern Precordillera has been associated with a thick-skinned style, similar to that of the Sierras Pampeanas (Zapata and Allmendinger, 1996). However, geological observations and seismic reflection data support the idea of thin-skinned structures detaching from Cambrian units, refolded by deeper basement structures, in agreement with models by Smalley et al. (1993). The front-end of the Precordillera seems to stop with a finite thickness at a suture on the eastern side of the Eastern Precordillera where the vergence inverts. The back-end of the Western Precordillera crust/lithosphere, geometry at the suture between the Chilenia and the Cuyania is largely unknown. In this work, we test the hypothesis of Pampean-style basement structures which are developing incipiently in the proximity and below the Precordillera.

Recent thermochronology studies carried out by Levina et al. (2014) in the south of Precordillera indicate that the deformation began at around 12–9 Ma. While Fosdick et al. (2015) using the same technique, indicate that the deformation started about of 18–14 Ma. The main deformation phase in Central Precordillera, peeking with large-scale exhumation, was at 12–9 Ma while the main phase in the Eastern Precordillera seems to have occurred at 6–2 Ma, in agreement with a recent study by Allmendinger and Judge (2014).

Topographic and fluvial relief data, cosmogenic analysis, variability of rainfall and discharge and crustal seismicity were used by Val et al. (2018) analyzing the tectonics versus the climatological components in the Precordillera. They proposed that the along-strike pattern of erosion rates in the southern Central Andes including the Precordillera is largely independent on climate and closely related to the shallow crustal seismicity and diachronous surface uplift. Val et al. (2018) analysis considered the crustal seismicity in the Precordillera as a whole; in this work we analyze the same seismicity with more detail in different inner parts of the Precordillera and its boundaries.

In this study, we relocate the crustal earthquake dataset presented in Val et al. (2018), testing for more seismic velocity models. We also estimate local and moment magnitudes as well as focal mechanisms. Our goal is to characterize the earthquake distribution beneath the Precordillera, detect regions of seismic clustering and estimate the regional stress orientations. Although earthquakes are more frequent and of higher magnitudes in the Sierras Pampeanas, there are records of historical earthquakes that have occurred in the Precordillera with large magnitudes such as the 1894 (M > 7) earthquake (INPRES, 2020; Rivas et al., 2019), the 1944 (M_w = 7.0) and 1952 (M_w = 6.8) earthquakes (Alvarado and Beck, 2006) (Fig. 1). These events suggest that the structure associated with the Precordillera may have the potential to generate moderate to large earthquakes as proposed by Smalley and Isacks (1990), although according to Smalley et al. (1993) basement structures would not be related to crustal faults reaching the surface. A better understanding of such structures is important for seismic hazard assessment. Association of those crustal faults with historical earthquakes is in an ongoing debate (Smalley et al., 1993; Alvarado and Beck, 2006). Modern patterns of earthquake deformation are unknown in the Precordillera and have inhibited interpretation of the fault geometries at depth for some of the exposed crustal faults. To investigate the possible association of seismicity to faulting structures or geometries, we analyze our earthquake hypocenters in the framework of the previous PANDA experiment results (Smalley et al., 1993) and the epicentral regions associated with the occurrence of historical earthquakes as well as regions with no historical earthquake records.

3. Data and methods

As a first step, we start with the previous seismic locations of Precordillera crustal earthquakes from Val et al. (2018) (Table S1) and relocate them using the JHD method to improve the locations. Val et al. (2018) obtained locations for a total of 100 crustal earthquakes (see Table S1) after applying quality criteria consisting of: (1) earthquakes recorded ≥30 seismological stations (2) an average of 37 phases of P- and S-wave arrivals for each earthquake determination; (3) epicentral errors < 2 km; (4) focal depth errors < 2.5 km; and (5) a root mean square of the difference between observed and calculated travel times (RMS) lower than 0.5 s. Val et al. (2018) earthquake locations and moment magnitudes M_w were calculated using the Seisan 10.3 software (Ottemöller et al., 2014). P-wave arrivals on the vertical component, and S-wave arrivals on the horizontal components were used in the seismic location process. Uncertainties in hypocentral determinations for those 100 earthquakes are due to possible picking errors and uncertainties in the seismic 1D velocity model (Ammirati et al., 2015) to calculate the predicted travel times.

In order to choose the seismic velocity model that best fits P- and S-wave arrivals we test the JHD relocations with three different models (Figs. 3, S1, S2, Table S2) available from previous studies: (1) The WSP model from Venerdini et al., 2016. This model describes the crustal velocity structure for the Cuyania terrane at ~31.5°S and ~68°W. Crustal thickness associated with this model is 47 km. (2) A regional model averaged from the joint inversion of receiver functions and surface wave dispersion in the Precordillera (Ammirati et al., 2015) and the Sierras Pampeanas (Ammirati et al., 2018). This model exhibits an average Moho depth of 50 km. (3) The regional model calibrated for the

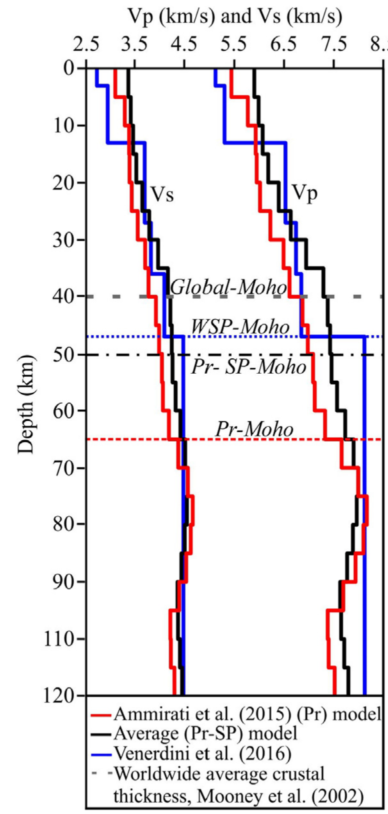

Fig. 3. Velocity models tested in this work. The corresponding Moho depth of each model is indicated as well as the average (global) Moho depth of 40 km by Mooney et al. (2002).

flab-slab region presented in Ammirati et al. (2015). The Moho for this model lies at 65 km depth.

The Moho depth associated with the velocity model proposed by Ammirati et al. (2015) is representative of the Precordillera sector and thus might be not optimal for analyzing the recorded in the ESP stations. However, omitting the phases from the ESP stations led to higher hypocentral uncertainties.

These models are showed in Fig. 3. We choose the velocity model proposed by Ammirati et al. (2015) for our subsequent analysis because it produced the most accurate results.

We perform a relocation of the 100 seismic events using the Joint-Hypocenter-Determination (JHD) program (Kissling et al., 1994) using the hypocenters from Val et al. (2018) as our starting locations. The JHD algorithm is included in the Seisan 10.3 package (Ottemöller et al., 2014). We also considered the available seismic-petrologic model by Ammirati et al. (2015), which was obtained from joint inversion of Rayleigh wave phase velocity dispersion and teleseismic receiver functions (Fig. 3) to determine the seismic relocations. The relocation considered the P- and S-wave arrival times and a damped least square inversion. As a result, hypocenters and their corresponding station delays are simultaneously estimated as well as possible variations to the seismic velocities for the 24-layer seismic velocity model following the methodology of Crosson (1976). We observe that the velocity model was slightly modified with maximum variations of 0.02 km/s. These variations produce a change of < 0.5 km (maximum) in epicenter locations and 1 km (maximum) in focal depths. Finally, we did the same process testing all of the four seismic velocity models in Fig. 3.

Local and moment magnitudes (M_L and M_w) were calculated for all seismic events. In order to determine the M_L magnitude, we generate a displacement trace in the frequency band 1.25–19.5 Hz and measure the maximum amplitude on the vertical component (Fig. 4a and b). As expected, the maximum amplitude occurs after the arrival of the S-wave

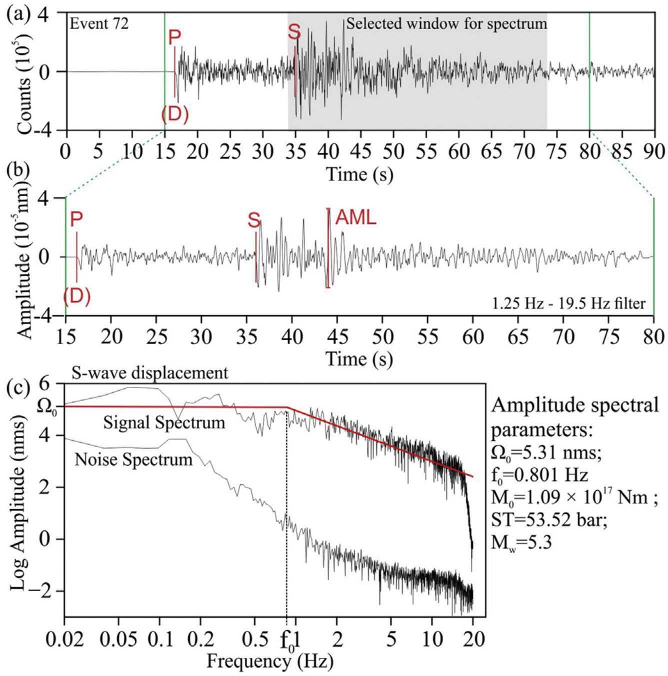

Fig. 4. (a) Vertical component seismogram corresponding to Event 72 on 2009-03-11 (Table S1) recorded at station NIKI (Fig. S1). Green bars indicate the time window selected for the calculation of M_L. The gray time window was used for the M_w estimation. The red lines indicate the first P- and S-wave arrivals and (D) denotes a downwards first motion. (b) Time window using a (Wood Anderson) filter between 1.25 Hz – 19.5 Hz for M_L calculation; AML denotes the maximum amplitude. (c) Example of M_w determination using the S-wave displacement spectrum and the noise spectrum for the same Event 72. The signal spectrum shows one flat component (Ω_0 = 5.31 nms) for lower frequencies, which is proportional to the seismic moment (M_0 = 1.09 × 10^{17} Nm); and another component obtained after the corner frequency (f_0 = 0.801 Hz), indicating an approximately linear decrease in amplitude of the spectrum for increasing frequency. Others parameters involved in the processing are: stress drop ST = 53.52 bar; source radius R = 2.2 km; S-wave velocity Vel = 4.5 km/s; density ρ = 3.4 gcm^{-3}; NIKI-source hypocentral distance dist = 151 km; Focal depth = 26.7 km; Regional attenuation Q_0 = 400; Local attenuation (Qalp = 0.7; k = 0.02); spectral frequency band = 0.010 Hz – 20 Hz. (For interpretation of the references to colour in this figure legend, the reader is referred to the web version of this article.)

for a local crustal earthquake. Then, M_L magnitude is defined by Richter (1935) as:

$$M_L = \log(AML) + Q_d \tag{1}$$

where AML is the maximum amplitude and Q_d is an epicentral distance correction function.

The calculation of the moment magnitude M_w (Fig. 4c) is determined by the spectral analysis after the arrival of the S-wave considering the following equation:

$$\mathrm{Mw} = \frac{2}{3}\log M_0 - 6.07 \tag{2}$$

where the M_0 is measured in Nm (Brune, 1970) and can be described as follows:

$$\mathrm{M_0} = \frac{\Omega_0 4\pi\rho v^3}{0.6 \times 2 \times \mathrm{G}(\Delta \mathrm{h})} \tag{3}$$

where Ω_0 is the flat level in the signal spectrum delimitated by the corner frquency f_0 (see Fig. 4c for one example), ρ (in gcm^{-3}) is the density, v (in kms^{-1}) is the S-wave velocity, the factor 0.6 accounts for an average radiation pattern effect, the factor 2 takes into account the effect of the free surface, G (Δ, h) is the geometrical spreading at an epicentral distance Δ (in km) and hypocentral depth h (in km). Thus, M_w is estimated for several seismic stations (about 35 in this study) for the same earthquake and averaged (Table S1). Fig. 4 shows an example of the local and moment magnitude calculations for Event 72, using the seismic station NIKI (more details can be obtained from Tables 1 and S1).

Then, we determined focal mechanisms using P-wave first motion polarities and the Focmec software (Snoke, 2003) considering the new takeoff angles from our relocated hypocenters (Table 1). In this methodology, positive (compressive) and negative (dilatational) polarities are observed at different backazimuths and epicentral distances. This information is represented on a lower hemisphere Lambert-Schmidt stereographic projection. A set of parameters consisting of strike, dip, and rake for two nodal planes are obtained by separating compressive from dilatational first motion arrivals. Because we are using local observations and a regionally calibrated velocity model as well as discarding doubtful polarity readings, we assumed zero polarity errors for the focal mechanism determinations. We used Aki and Richards (1980) convention to report the fault plane solutions in Tables 1 and S1. We calculated 100 focal mechanisms for the relocated seismicity beneath the Precordillera.

P- and T- axis from our focal mechanism solutions were inverted to estimate the regional stress tensor based on the probabilistic formulation of the right trihedral method (using a Matlab program from D'Auria and Massa, 2015). This method allows a quantitative estimation of the confidence regions for the principal stress axes where σ_1 is the maximum (compressive) principal stress and σ_3 is the minimum (tensional) principal stress (Stacey and Davis, 2008).

4. Results

4.1. Earthquake relocations and magnitude determination

Figs. 5a and b show the differences between original locations by Val et al. (2018) and our JHD relocations for each seismic event in this study. Fig. 5c summarizes the differences between located and relocated hypocenters in terms of depth, latitude and longitude. The major difference is observed for the focal depth with an average offset of −1.5 ± 2.5 km (one standard deviation). Differences in latitude and longitude are 0.6 ± 1.6 and -− 2.9 ± 1.7, respectively. In general, we do not observe significant differences in terms of epicenters between located and relocated events. In addition, the relocated hypocenters appear more clustered in some sectors, which allows further tectonic interpretations. The parameters that characterize the relocated and located earthquakes are shown in Tables 1 and S1, respectively. In general, the seismicity is observed between 6 km and 50 km depth within the crust, extending to abnormally deep levels of a continental crust (e.x. Smalley and Isacks, 1990; Smalley et al., 1993; Richardson et al., 2012; Pérez et al., 2015; Ammirati et al., 2015).

Magnitude estimations for the Precordilleran crustal earthquakes indicate small-to-moderate sizes with values 0.4 ≤ M_L ≤ 5.3 corresponding to estimations of 1.3 ≤ M_w ≤ 5.3 reported in Val et al. (2018) (Tables 1 and S1). We observed that M_L is lower than M_w (Fig. S3), which is consistent with suggestions by Sánchez et al. (2013) for the same region using a different dataset and by Bethmann et al. (2011) in Switzerland for local earthquakes. Relatively deeper crustal earthquakes would produce more attenuation in the S-wave amplitude record at a specific station where M_L is calculated in comparison to shallower events that produce higher amplitude S-waves and thus, higher M_L. For this reason, the moment magnitude M_w is a better estimation of the magnitude, regardless of the size of the earthquake.

4.2. Focal mechanisms

After obtaining new relocation results for the 100 crustal earthquakes we obtained new focal mechanisms (Table 1 and Fig. 6) and compared them with previous determined focal mechanisms

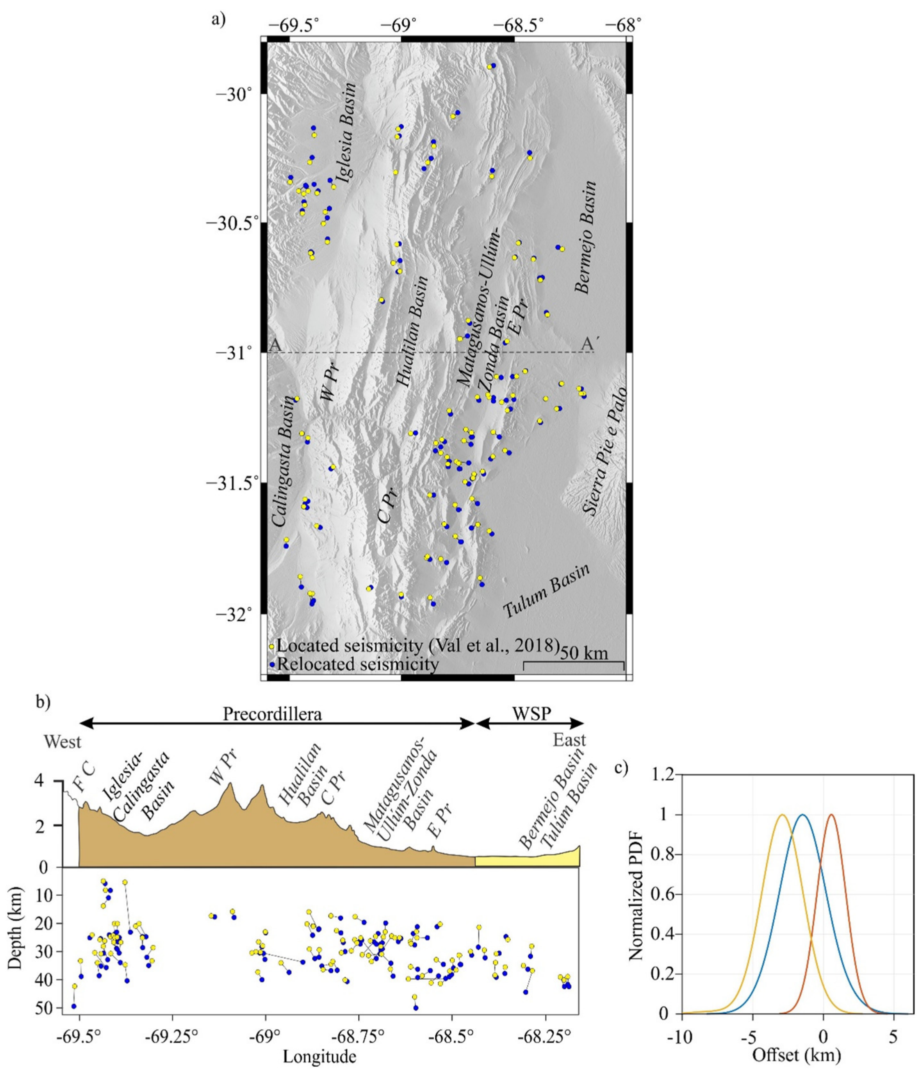

Fig. 5. (a) Relocated (blue dots) in comparison with previous locations (yellow dots) from Val et al. (2018). A-A′ represents the location of the cross-section shown in (b); other morphostructural units are as in Fig. 1. (b) Cross-section at ~31°S showing the depth distribution of both relocated and previously located events. (c) Normalized probability density function showing the differences in latitude (red), longitude (yellow) and depth (blue) between located and relocated earthquakes; overall earthquakes lie at deeper levels, eastern and northern after relocation using Ammirati et al. (2015) model in Fig. 3. (For interpretation of the references to colour in this figure legend, the reader is referred to the web version of this article.)

corresponding to seismic locations in Val et al. (2018) (Table S1). After relocation, our results indicate 22 reverse focal mechanism solutions, 24 mainly reverse solutions with some minor strike-slip component, 19 left-lateral strike-slip solutions with a minor reverse component, 5 left-lateral strike-slip solutions, 13 left-lateral strike-slip solutions with minor normal components and 17 normal solutions with some minor strike-slip component (Table 1 and Fig. 6). We note that the differences between the focal mechanisms from Val et al. (2018) and those obtained from relocation in this work do not present significant differences. Therefore we do not expect radical changes in terms tectonic interpretations. An example is shown in Fig. 7, for the Seismic Event 1 in Table 1 with M_L 3.5 and M_w 3.7 that occurred on 23 January 2008. The same figure shows six stations with compressive P-wave first arrival motion (indicated as “C” using blue circle symbols); whereas 19 stations exhibit a clear dilatational P-wave first arrival motion (denoted as “D” and red triangle symbols).

Compressional P, tensional T, and null B axis (Isacks and Molnar, 1971) combination for each solution has been then plotted according to the method described by Frohlich (1992, 2001); this helps to clearly identify the diversity of focal mechanisms obtained. Fig. 8 shows the normalized density of focal mechanism distribution for the relocated earthquakes (Table 1).

P- and T-axis inversion of our 100 relocated crustal earthquakes yielded regional stress axis orientations. The maximum stress axis (σ_1) exhibits an 85° strike and a 7.2° plunge angle. The minimum stress (σ_3) is almost vertical with a plunge angle of 82.3° (Fig. 9).

5. Discussion

The crustal seismicity recorded during 2008 and 2009 above the flat subduction of the Nazca plate in the Argentine retroarc region of the Precordillera, has a distribution with depths between 6 km and 50 km. The hypocenters determined in this work show greater depths than those observed for the seismicity from PANDA experiment between 5 km and 35 km depth (Smalley and Isacks, 1990; Smalley et al., 1993) and those proposed by Val et al. (2018) between 5 km and 46 km depth. Thus, the observed seismicity is deep compared to depths expected for a typical granite continental crust where the brittle-ductile transition may be at 15–20 km (Alvarado et al., 2005). Observations from Pérez et al. (2015) and Castro de Machuca et al. (2012) definitively show the mafic character of the Cuyania crust, which suggests a brittle-ductile transition occurring at greater depths. Smalley and Isacks (1990) suggested a brittle-ductile transition at about 30 km–35 km depth.

Our seismic source results beneath the Precordillera and the Iglesia-Calingasta Basin agree with thickening of middle-to-lower crustal levels; this has been also observed by previous local studies (Alvarado et al., 2009b; Ammirati et al., 2015; Rivas et al., 2019).

Three large historical damaging earthquakes of magnitudes greater than $M_w >$ 6.8 were located in the Precordillera (Alvarado and Beck, 2006; INPRES, 2020) (Fig. 1). We observe other small-to-moderate crustal events in the same epicentral regions (Fig. 6a). In order to analyze a possible association between past and modern seismic activity zones in more detail, we made four cross-sections in the northern

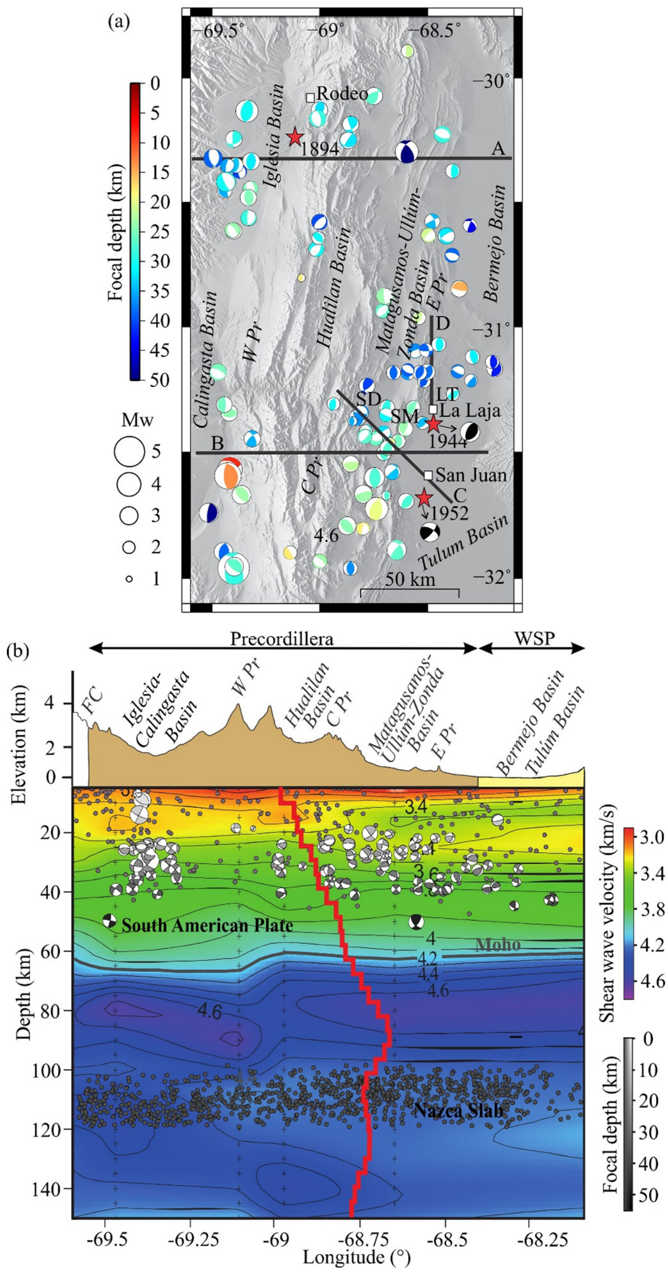

Fig. 6. (a) Focal mechanism solutions obtained in this study following Aki and Richard's (1980) convention for their representation. Different colors of the compressive quadrants denote focal depths. "A", "B", "C" and "D" indicate the locations of the corresponding cross-sections shown in a figure below. Historical earthquakes (red stars) are also shown including the 1894 event (Rivas et al., 2019) as well as the 1944 and 1952 events with their focal mechanisms (Alvarado and Beck, 2006). Precordilleran ranges are SD: Sierra de La Dehesa, SM: Sierra de Matagusanos and LT: Loma de las Tierritas; other units as in Fig. 1. (b) Cross section at ~31°S showing our focal mechanism solutions projected along the cross-section plane. The size of beach balls is related to the magnitude (1.3 < M_w < 5.3). Dots are seismic events from the ISC catalog (2000–2017). Lithospheric shear-wave variations obtained by Ammirati et al. (2015) are shown in the background. The seismic velocity model for the Precordillera used in our study is plotted in red solid line. Major geologic units refer to the main text and are the same as in Fig. 1. (For interpretation of the references to colour in this figure legend, the reader is referred to the web version of this article.)

(cross-section A) and southeastern (cross-sections B, C and D) Precordillera sectors (Figs. 6a and 10).

Overall, cross-section A (Figs. 6a and 10a) in the northern sector, shows focal mechanisms with steep fault plane solutions. To the west beneath the Iglesia Basin, we observe seismicity with hypocentral depths between 20 km and 40 km and faulting solutions with an approximate north-south strike. This seismicity is interpreted as the presence of a major north-south ramp dipping to the west and connecting deep structures of the Frontal Cordillera with the old thin-skinned system of the Western Precordillera, consistent with interpretations from Rivas et al. (2019).

Focal mechanisms in this sector indicate compression in an almost E-W orientation at middle-to-lower crust levels. However, there is evidence of recent tectonic activity such as stream channel offsets within Quaternary fan deposits (Bastías and Uliarte, 1991; Siame et al., 1996) along the central segment of the El Tigre fault (Western Precordillera, ~30.3°W); that suggest a transpressive component in the deformation of the upper crust and at the transition between the Frontal Cordillera (Chilenia) and the Western Precordillera (Cuyania). In the eastern part of cross-section A, the seismicity is located between 20 km and 50 km depths and seems to follow preferential west-dipping planes, inferred between 20 and 40 km depths (Fig. 10a). The easternmost plane could connect with the east-dipping décollement that separates the Eastern Precordillera from the Western Sierras Pampeanas. Interestingly, Smalley et al. (1993) formerly proposed a similar idea for the region located about 100 km southward (~31.5°S, Fig. 10c). Our observations strengthen Smalley et al.'s (1993) hypothesis and suggest a continuity of this structure from north to south for about 70 km horizontal distance.

Geological observations along 30°S indicate that shallow (0 to 20 km depths) thin-skinned deformation regime dominated in the Precordillera approximately 10 Ma with estimations of an E-W shortening of total ~ 86 km ± 22 km (Allmendinger and Judge, 2014). However, our seismicity evidences crustal shortening at middle-to-lower crust levels, hence suggesting ongoing thick-skinned deformation within the Cuyania basement.

More to the south, around ~31.5°S (cross-section B, Figs. 6a and 10b) similar features can be observed. In the western section (~69.5°W), the transition between the Frontal Cordillera and the Western Precordillera shows seismicity along west dipping structures with reverse focal mechanisms in good agreement with receiver function observations by Ammirati et al. (2016). More to the east, and similarly to cross-section A (Fig. 10a) the seismicity seems to align along west dipping faulting structures, confirming the thick-skinned character of the Cuyania basement deformation. A more detailed cross-section (Fig. 10c) focuses on the transition between the Eastern Precordillera and the Western Sierras Pampeanas where Smalley et al. (1993) formerly worked. In general, our seismicity is consistent with that one from the PANDA experiment analyzed by Smalley et al. (1993) but allow to interpret the structure responsible for the deformation of the Cuyania basement extending farther to the west.

In detail, cross-section C (Figs. 6a and 10c) also allowed us to compare our seismic relocation results with those from the previous PANDA experiment (Smalley et al., 1993). Our hypocenters are distributed along a blind fault striking ~45° and dipping ~35° to the northwest; we call this structure the *Smalley Fault* (SF) and it is shown in Fig. 10c. We note that the 1944 (M_w7.0) and the 1952 (M_w6.8) earthquakes (Alvarado and Beck, 2006) (Fig. 6a) exhibit hypocenters at about 10 km depth, this could coincide with structures above the SF. Field observations of surface ruptures after the 1944 "La Laja" (M_w 7.0) earthquake, were compatible with the activation of an east-dipping fault (Alvarado and Beck, 2006), rather than the SF.

The cross-section C shows to the southeast of the SF, a more diffuse seismicity pattern between 20 and 40 km depths, at lower crustal levels which is in agreement with observations of earthquake activity in the Cuyania basement probably responsible for the uplift of the Sierra Pie de Palo and Sierra Valle Fértil-La Huerta in the Western Sierras Pampeanas (Regnier et al., 1992; Smalley et al., 1993; Ramos et al., 2002; Monsalvo et al., 2014). In addition, there are more earthquakes

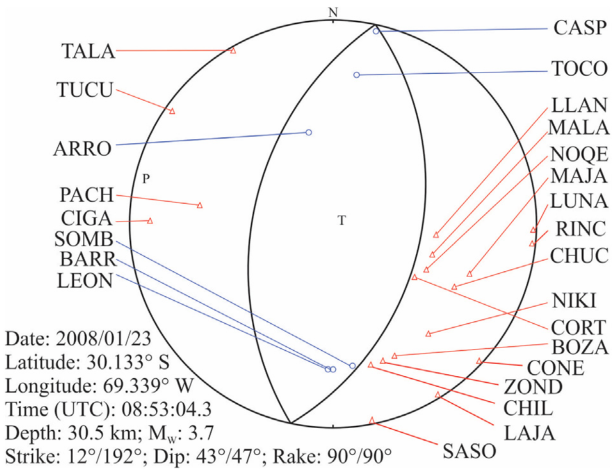

Fig. 7. Example of a focal mechanism corresponding to Event 1 (Table 1) obtained using Focmec (Snoke, 2003). Blue circles indicate compressional (C) P-wave arrivals and red triangles dilatational (D) P-wave arrivals associated to the four-letter labeled stations used for the calculation (http://www.fdsn.org/networks/detail/ZL_2007/). T and P show the tension and pressure axes. (For interpretation of the references to colour in this figure legend, the reader is referred to the web version of this article.)

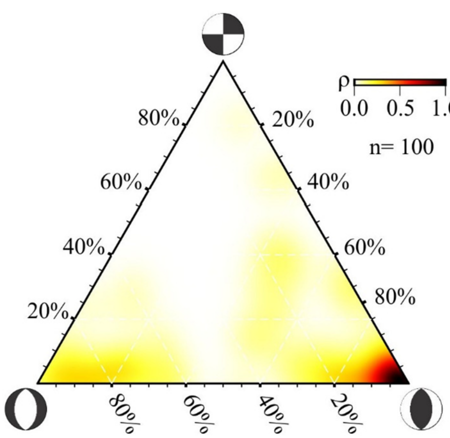

Fig. 8. Triangular diagram showing normalized density (ρ) of focal mechanism distribution (Frohlich, 1992, 2001). Note that most of our solutions correlate with a higher probability density of reverse focal mechanisms.

between 14 km and 34 km, which occur in structures adjacent and to the southeast of the SF, which has been also detected by Smalley et al. (1993).

Cross-section D (Figs. 6a and 10d) was chosen with a similar N-S orientation as in Smalley et al.'s (1993) study. Our earthquake depth distribution coincide with the seismic structure dipping to the south observed by Smalley et al. (1993) between 31°S and 31.5°S. Our focal mechanism solutions in this sector, however, show reverse faulting with a north-northeast orientation, compatible with other regional structures exposed at the surface (Costa et al., 2000; Alvarado and Sáez, 2006).

In general, the focal mechanisms obtained in this work are consistent with E-W compression (Fig. 8). This suggests crustal shortening contributing to the thickening and uplifting of the Precordillera. All earthquake depth determinations are at the middle-to-lower crust levels, clearly suggesting that the basement of the Precordillera is active below its upper thin-skinned levels (Jordan et al., 1983; Zapata and Allmendinger, 1996), thus providing evidence for shallow thin-skinned deformation that precedes this modern basement deformation.

Fosdick et al. (2015) have used low-temperature thermochronological techniques involving apatite (U-Th-Sm/He) and fission track and suggested that the Precordillera began to get exhumed 18 Ma,

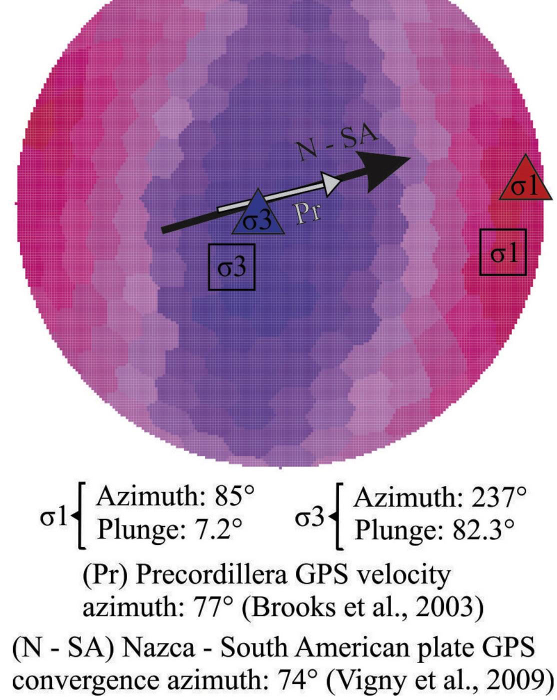

Fig. 9. Regional stress tensor representation from the inversion of our 100 focal mechanism solutions (Fig. 6 and Table 1). The red and blue triangles indicate the projection on the focal shpere of the maximum (σ_1) and minimum (σ_3) main stresses (D'Auria and Massa, 2015). The black arrow shows the Nazca-South American plate convergence orientation (Vigny et al., 2009). The white arrow shows the GPS velocity azimuth in the Precordillera (Brooks et al., 2003). The gray square indicates the locations of the maximum horizontal σ_1 and minimum vertical σ_3 main stresses from Val et al. (2018). (For interpretation of the references to colour in this figure legend, the reader is referred to the web version of this article.)

from west to east as a result of shallow thin-skinned deformation (Precordillera fold and thrust belt). Modern seismicity obtained in this study indicates that the Central Precordillera fold and thrust belt is currently silent, thus not accommodating crustal shortening. However, the Precordillera basement would be currently accommodating shortening by thick-skinned deformation along west-dipping crustal structures rooted at about 40 km depth, in the Cuyania basement (Fig. 11). This feature seems to present a good continuity from north (~30°S) to south (~32°S) although, the seismic activity is slightly more frequent and of higher magnitude in the south of our study region. In particular, relatively large magnitude earthquakes in this study have been characterized beneath the Calingasta basin (Fig. 6a and Table 1), at the transition between Cuyania and Chilenia.

This crustal deformation may be a good model to explain the abnormally thick Cuyania crust (> 60 km beneath the Precordillera) by thrusting large sections of the basement (Alvarado et al., 2010; Ammirati et al., 2015).

Interestingly, the projection of the JFR on the continent (see Fig. 1) coincides with this southern sector. This region above the flat slab subduction of the Nazca plate generates more crustal deformation in this sector than it does more to the north, as previously observed by Smalley et al. (1993). Actually, processes linking the flat slab subduction at ~100 km depth and the crustal deformation are still not fully understood.

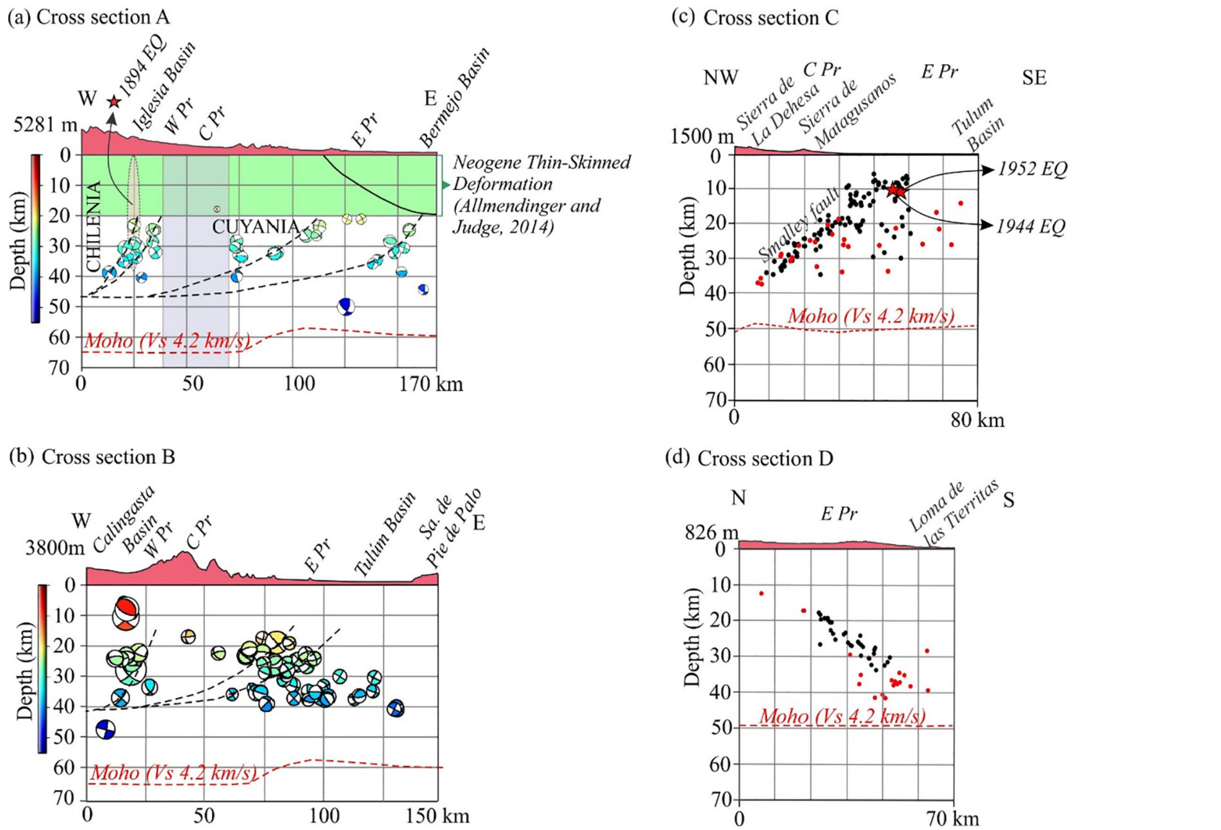

Fig. 10. Regional cross-sections shown in Fig. 6a. (a) Cross-section A for the northern Precordillera sector showing focal mechanisms (Table 1) in vertical projection along the cross-section. Note the higher concentration of earthquakes at the transition between the Cuyania and Chilenia terranes, which correlates with the 1894 historical earthquake epicentral area (oval). Also note the cluster of events deep into the Cuyania basement along two possible west-dipping planes. The thin-skinned deformation area suggested by Allmendinger and Judge (2014) is in the upper part in green. (b) Same as (a) but for the southern Precordillera (see location in Fig. 6a). Similar interpretations can be made in comparison to results for the northern cross-section A, although the seismicity in the south seems more numerous. (c) Cross-section C (see location in Fig. 6a) showing our seismicity (Table 1) as red dots and a comparison with hypocenters from the PANDA (1987–1988) determinations (Smalley et al., 1993) as black dots, beneath the Central and Eastern Precordillera. Note how the seismicity is aligned along a blind fault structure of an azimuth of ~45° and dipping 35° to the west (the *Smalley fault)*. The seismicity in this area also correlates with the historical 1944 and 1952 earthquake epicentral areas (Alvarado and Beck, 2006). (d) Cross-section D showing another comparison between our results and those from the PANDA experiment. Note the good correlation defining a fault of azimuth 86° and dip of about 30° to the south.
In all cross-sections, the dashed red lines represent the average Moho estimated from S-wave velocity observations (Vs = 4.2 km/s, see Fig. 3) (Ammirati et al., 2015). (For interpretation of the references to colour in this figure legend, the reader is referred to the web version of this article.)

6. Conclusions

We relocated 100 crustal earthquakes in the Precordillera region above the flat-slab segment in the Andean retroarc of Argentina using the JHD method. Our estimations of local earthquake magnitudes indicate small-to-moderate sized seismic sources with $0.4 \le M_L \le 5.3$ and $1.3 \le M_w \le 5.3$. Hypocenter relocations are mainly distributed between 25 km and 35 km depths. We note that this seismicity during 2008 and 2009, is mainly located in regions along the Iglesia-Calingasta Basin and the Eastern Precordillera with a more quiet Central Precordillera. The focal mechanisms mostly agree with reverse motion of north-south trending structures. The estimation of the principal stress orientations shows a nearly horizontal maximum stress (σ_1) with an azimuth of 85° and a nearly vertical minimum stress (σ_3), which is consistent with middle-to-lower crust E-W compression. The seismicity characterized in this work is compatible with thick-skinned

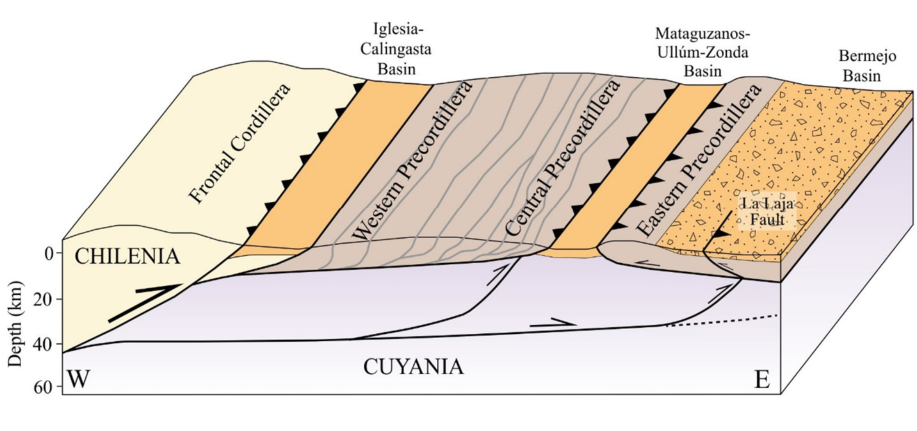

Fig. 11. Schematic block representation of the continual crust in our study region showing the main units (as in Fig. 1), faulting structures exposed at the surface (Perucca and Vargas, 2014; Costa et al., 2015a, 2015b, 2018) as well as the structures inferred from the seismicity characterized in this study. The arrows are associated with currently active (seismic) structures. Note that the thin-skinned deformed Central and Western Precordillera structures do not exhibit modern seismicity. The Cuyania basement accomodates crustal shortening by thick-skinned deformation rooted at a middle crustal level (~40 km).

deformation beneath the Precordillera in the Cuyania basement at middle-to-lower crustal levels; in this sense, there is a good correlation between our results using broandband dense SIEMBRA and ESP (2008–2009) networks and the previous (1987) PANDA short period network. Our results provide evidence for a seismically active basement beneath the previously deformed Precordillera. This thin-skinned deformation mostly pre-date the present basement deformation inferred in this work. The abnormally deep seismicity beneath the Precordilleran earthquakes argues for a brittle lower crust probably related to the mafic character of the Cuyania basement and possibly to the flat slab processes.

Supplementary data to this article can be found online at https://doi.org/10.1016/j.tecto.2020.228450.

Declaration of competing interest

None.

Acknowledgements

We thank the IRIS-PASSCAL SIEMBRA and ESP experiments that provided the seismic data (NSF, EAR 0510966 USA). Financial support for this study came from the Permanent Program at the UNSJ "Sismicidad Andina utilizando una Red Sismológica de Banda Ancha" (Res. 100/2008-CEFN), and Projects PICT2016-0046 and PICT2017-0676, PDTS 80020150600009SJ and PROJOVI 10120180400037SJ, Res No 1119/18-R-UNSJ). Maps were generated using Generic Mapping Tools (Wessel and Smith, 1991). The authors are grateful to Mauro Sáez and the Grupo de Sismotectónica (CIGEOBIO-CONICET). Comments from the editor and Robert Smalley have greatly contributed to improve this work.

References

Aki, K., Richards, P., 1980. Quantitative Seismology. Theory and Methods. Freeman, San Francisco.

Allmendinger, R., Judge, P., 2014. The Argentine Precordillera: a foreland thrust belt proximal to the subducted plate. Geosphere 10 (6), 1203–1218. https://doi.org/10.1130/GES01062.1.

Allmendinger, R., Figueroa, D., Snyder, D., Beer, J., Mpodozis, C., Isacks, B., 1990. Foreland shortening and crustal balancing in the Andes at 30°S latitude. Tectonics 9 (4), 789–809. https://doi.org/10.1029/TC009i004p00789.

Alonso, J.L., Gallastegui, J., García-Sansegundo, J., Farías, P., Rodríguez Fernández, L.P., Ramos, V., 2008. Extensional tectonics and gravitational collapse in an Ordovician passive margin: the Western Argentine Precordillera. Gondwana Res. 13, 204–215. https://doi.org/10.1016/j.gr.2007.05.014.

Alvarado, P., Beck, S., 2006. Source characterization of the San Juan (Argentina) crustal earthquakes of 15 January 1944 (M_W 7.0) and 11 June 1952 (M_W 6.8). Earth Planet. Sci. Lett. 243 (3–4), 615–631. https://doi.org/10.1016/j.epsl.2006.01.015.

Alvarado, P., Castro de Machuca, B., Beck, S., 2005. Comparative seismic and petrographic crustal study between the Western and Estern Sierras Pampeanas region (31°S). Rev. Asoc. Geol. Argent. 60 (4), 787–796.

Alvarado, P., Sáez, M., 2006. Estudio sismológico e histórico del terremoto de San Juan, Argentina, del 15 de enero de 1944. Anales de la Academia Nacional de Ciencias Exactas, Físicas y Naturales. 58, 79–92.

Alvarado, P., Pardo, M., Gilbert, H., Miranda, S., Anderson, M., Saez, M., Beck, S.L., 2009b. Flat-slab subduction and crustal models for the seismically active Sierras Pampeanas región of Argentina. In: Kay, S., Ramos, V.A., Dickinson, W. (Eds.), Backbone of the Americas: Shallow Subduction, Plateau Uplift, and Ridge and Terrane Collision: Boulder, Colorado, Geological Society of America, Memoria. 204. pp. 261–278.

Alvarado, P., Saez, M., Araujo, M., Perarnau, M., Guell, A., Gregori, D., Sánchez, G., 2009a. Experimento Geofísico SIEMBRA: más detalles de la subducción plana en Argentina y la deformación en la placa superior. 14° Reunión de Tectónica, Río Cuarto, Córdoba, Argentina.

Alvarado, P., Sánchez, G., Saez, M., Castro de Machuca, B., 2010. Nuevas evidencias de la actividad sísmica del terreno Cuyania en la región de subducción de placa horizontal de Argentina. Revista Mexicana de Ciencias Geológicas 27 (2), 278–291.

Ammirati, J., Alvarado, P., Beck, S., 2015. A lithospheric velocity model for the flat slab region of Argentina from joint inversion of Rayleigh wave phase velocity dispersion and teleseismic receiver functions. Geophys. J. Int. 202, 224–241. https://doi.org/10.1093/gji/ggv140.

Ammirati, J., Pérez, S., Alvarado, P., Beck, S., Rocher, S., Zandt, G., 2016. High-resolution images above the Pampean flat slab of Argentina (31–32°S) from local receiver functions: implications on regional tectonics. Earth Planet. Sci. Lett. 450, 29–39. https://doi.org/10.1016/j.epsl.2016.06.018.

Ammirati, J.B., Venerdini, A., Alcacer, J.M., Alvarado, P., Miranda, S., Gilbert, H., 2018. New insights on regional tectonics and basement composition beneath the eastern Sierras Pampeanas (argentine back-arc region) from seismological and gravity data. Tectonophysics 740, 42–52. https://doi.org/10.1016/j.tecto.2018.05.015.

Amos, A.J., 1972. Las cuencas carbónicas y pérmicas de Argentina. Anais Academia Brasileira Ciencias, (Supl.). 44, 21–30.

Amos, A.J., Rolleri, E.O., 1965. El Carbónico marino en el valle Calingasta - Uspallata (San Juan - Mendoza). Boletín de Informaciones Petroleras 368, 50–71.

Anderson, M., Alvarado, P., Zandt, G., Beck, S., 2007. Geometry and brittle deformation of the subducting Nazca plate, central Chile and Argentina. Geophys. J. Int. 171 (1), 419–434. https://doi.org/10.1111/j.1365-246X.2007.03483.x.

Anselmi, G., Cegarra, M., Gaido, F., 2006. Hoja Geológica 3169–27 Barreal. Escala 1:100.000 Servicio Geológico Minero Argentino. Informe inédito.

Baldis, B., Bordonaro, O., 1984. Cámbrico y Ordovícico de la Sierra Chica de Zonda y Cerro Pedernal, provincia de San Juan, Génesis del margen continental de la Precordillera. In: 9° Congreso Geológico Argentino, Bariloche, Río Negro, Argentina, 4, pp. 190–207.

Baldis, B., Chebli, G., 1969. Estructura profunda del área central de la Precordillera sanjuanina. Jornadas Geológicas Argentinas 1 (4), 47–65.

Barazangi, M., Isacks, B., 1976. Spatial distribution of earthquakes and subduction of the Nazca plate beneath South America. Geology 4 (11), 686–692. https://doi.org/10.1130/0091-7613(1976)4<686:SDOEAS>2.0.CO;2.

Barredo, S.P., Ramos, V., 2009. Características tectónicas y tectosedimentarias del hemigrben Rincón Blanco: Una Síntesis. Rev. Asoc. Geol. Argent. 66 (1), 133–145.

Bastías, J.A., Uliarte, E., 1991. Tectoformas de transcurrencia, falla El Tigre, sector central, San Juan. In: 6° Congreso Geológico Chileno, Resúmenes expandidos, pp. 506–509 Viña del Mar, Chile.

Beck, S., Zandt, G., 2007. Lithospheric structure and deformation of the flat slab region of Argentina. In: International Federation of Digital Seismograph Network. Data/Seismic Network, https://doi.org/10.7914/SN/ZL_2007.

Beer, J.A., 1989. Magnetic Polarity Stratigraphy and Depositional Environments of the Bermejo Basin, and Seismic Stratigraphy of the Iglesia Basin, Central Andes. Thesis of PhD. Cornell University, Ithaca, pp. 1–195.

Beer, J.A., Allmendinger, R., Figueroa, D., Jordan, T., 1990. Seismic stratigraphy of a Neogene piggyback basin, Argentina. Am. Assoc. Pet. Geol. Bull. 74, 1183–1202. https://doi.org/10.1306/0C9B244D-1710-11D7-8645000102C1865D.

Bethmann, F., Deichmann, N., Mai, P., 2011. Scaling relations of local magnitude versus moment magnitude for sequences of similar earthquakes in Switzerland. Bull. Seismol. Soc. Am. 101 (2), 515–534. https://doi.org/10.1785/0120100179.

Bollinger, G.A. and. Langer, C.J., 1988. Aftershocks of the western Argentina (Caucete) earthquake of 23 November 1977: some tectonic implications. Tectonophysics. Volume 148, issues 1–2, pages 131–146. ISSN 0040-1951. doi:https://doi.org/10.1016/0040-1951(88)90166-7.

Brooks, B.A., Bevis, M., Smalley Jr., R., Kendrick, E., Manceda, R., Lauría, E., Maturana, R., Araujo, M., 2003. Crustal motion in the Southern Andes (26°–36° S): do the Andes behave like a microplate? Geochem. Geophys. Geosyst. 4 (10). https://doi.org/10.1029/2003GC000505.

Brune, J., 1970. Tectonic stress and seismic shear wave from earthquakes. J. Geophys. Res. 75, 4997–5009. https://doi.org/10.1029/JB075i026p04997.

Cahill, T., Isacks, B., 1992. Seismicity and shape of the subducted Nazca plate. J. Geophys. Res. 97 (B12), 17503–17529. https://doi.org/10.1029/92JB00493.

Caminos, R., 1979. Cordillera Frontal: Córdoba. In: Castellanos, T.G., Sersic, J.L., Amuchastegui, S., Caputto, R., Cocucci, A.E., Fuchs, G.L., Gordillo, C.E., Melo, C.R. (Eds.), 2° Simposio de Geología Regional Argentina. 1. Academia Nacional de Ciencias, Córdoba, Argentina, pp. 397–453.

Castro de Machuca, B, Perarnau, M., Alvarado, P., López, M., Sáez, M., 2012. A seismological and petrological crustal model for the Southwest of the Sierra de Pie de Palo, province of San Juan. Revista de la Asociación Geológica Argentina 69 (2), 177–184.

Chiu, J.M., Steiner, G., Smalley, R., Johnston, A.C., 1991. PANDA: a simple, portable seismic array for local-to regional-scale seismic experiments. Bull. Seismol. Soc. Am. 81 (3), 1000–1014.

Cortés, J.M., 1993. El frente de corrimiento de la Cordillera Frontal y el extremo sur del valle de Uspallata, Mendoza. In: Ramos, V. (Ed.), 17° Congreso Geológico Argentino y II Congreso de Exploración de Hidrocarbouros, Buenos Aires, Argentina, pp. 168–178.

Costa, C., Machette, M., Dart, R., Bastias, H., Paredes, J., Perucca, L., Tello, G., Haller, K., 2000. Map and database of Quaternary faults and folds in Argentina. US Geological Survey Open-File Report 108, 75. https://doi.org/10.1029/1999GL006087.

Costa, C.H., Ahumada, E.A., Vázquez, F.R., Kröhling, D.M., 2015a. Holocene shortening rates of an Andean-front thrust, Southern Precordillera, Argentina. Tectonophysics 664, 191–201. https://doi.org/10.1016/j.tecto.2015.09.017.

Costa, C.H., Ahumada, E.A., Gardini, C.E., Vázquez, F.R., Diederix, H., 2015b. Quaternary shortening at the orogenic front of the Central Andes of Argentina: the Las Penas Thrust System. Geol. Soc. Lond., Spec. Publ. 399 (1), 245–266. https://doi.org/10.1144/SP399.5.

Costa, C.H., Owen, L.A., Ricci, W.R., Johnson, W.J., Halperin, A.D., 2018. Holocene activity and seismogenic capability of intraplate thrusts: Insights from the Pampean Ranges, Argentina. Tectonophysics 737, 57–70. https://doi.org/10.1016/j.tecto.2018.05.002.

Cristallini, E.O., Ramos, V.A., 2000. Thick-skinned and thin-skinned thrusting in the La Ramada fold and thrust belt: crustal evolution of the High Andes of San Juan, Argentina (32 SL). Tectonophysics 317 (3–4), 205–235. https://doi.org/10.1016/S0040-1951(99)00276-0.

Crosson, R., 1976. Crustal structure modelling of earthquake data, 1, Simultaneus last squares estimation of hypocenter and velocity parameters. J. Geophys. Res. 81,

3036–3046. https://doi.org/10.1029/JB081i017p03036.
D'Auria, L., Massa, B., 2015. Stress inversion of focal mechanism data using a Bayesian Approach: a novel formulation of the Right Trihedra Method. Seismol. Res. Lett. 86, 1–10. https://doi.org/10.1785/0220140153.
Davis, J.S., Roeske, S.M., McClelland, W.M. y Kay, S.M., 2000. Mafic and ultramafic crustal fragments of the SW Precordillera terrane and their bearing on tectonic models of the early Paleozoic in W-Argentina. Geology 28: 171–174. (doi:10.1130/0091-7613(2000)28 < 171:MAUCFO > 2.0.CO;2).
Fosdick, J.C., Carrapa, B., Ortíz, G., 2015. Faulting and erosion in the Argentine Precordillera during changes in subduction regime: Reconciling bedrock cooling and detrital records. Earth Planet. Sci. Lett. 432, 73–83. https://doi.org/10.1016/j.epsl.2015.09.041.
Frohlich, C., 1992. Triangle diagrams: ternary graphs to display similarity and diversity of earthquake focal mechanisms. Phys. Earth Planet. Inter. 75 (1–3), 193–198. https://doi.org/10.1016/0031-9201(92)90130-N.
Frohlich, C., 2001. Display and quantitative assessment of distributions of earthquake focal mechanisms. Geophys. J. Int. 144 (2), 300–308. https://doi.org/10.1046/j.1365-246x.2001.00341.x.
Furque, G., González, P., Caballé, F., 1999. Hoja Geológica San José de Jáchal (Informe preliminar). In: In: Servicio Geológico Minero Argentina, Boletín 279, Buenos Aires, Argentina, pp. 52.
Gans, C., Beck, S., Zandt, G., Gilbert, H., Alvarado, P., Anderson, M., Linkimer, L., 2011. Continental and oceanic crustal structure of the Pampean flat slab region, western Argentina, using receiver function analysis: new high-resolution results. Geophys. J. Int. 186, 45–58. https://doi.org/10.1111/j.1365-246X.2011.05023.x.
Gilbert, H., 2008. Lithospheric Structure above the variably dipping Nazca Slab. In: International Federation of Digital Seismograph Networks. Other/Seismic Network, https://doi.org/10.7914/SN/XH_2008.
Gilbert, H., Beck, S., Zandt, G., 2006. Lithospheric and upper mantle structure of central Chile and Argentina. Geophys. J. Int. 165 (1), 383–398. https://doi.org/10.1111/j.1365-246x.2006.02867.x.
González, C.R., 1985. Esquema bioestratigráfico del Paleozoico superior marino de la Cuenca Uspallata-Iglesia, República Argentina. Acta Geológica Lilloana 16 (2), 231–244.
Heredia, N., Rodríguez Fernández, L.R., Gallastegui, G., Busquets, P., Colombo, F., 2002. Geological setting of the Argentine Frontal Cordillera in the flat-slab segment (30°00′–31°30′S latitude). J. S. Am. Earth Sci. 15 (1), 79–99. https://doi.org/10.1016/S0895-9811(02)00007-X.
INPRES, 2020. Instituto Nacional de Prevencion Sismica. www.inpres.gob.ar.
Isacks, B., Barazangi, M., 1977. Geometry of Benioff zones: lateral segmentation and downwards bending of the subducted lithosphere. Maurice Ewing Series 99–114. https://doi.org/10.1029/me001p0099.
Isacks, B., Molnar, P., 1971. Distribution of stresses in the descending lithosphere from a global survey of focal-mechanism solutions of mantle earthquakes. Rev. Geophys. 9 (1), 103–174. https://doi.org/10.1029/RG009i001p00103.
ISC, 2020. International Seis*mological Center,* On-line Bulletin. http://www.isc.ac.ukInternational Seismological Centre, Thatcham, United Kingdom.
Jordan, T.E., Isacks, B.L., Allmendinger, R.W., Brewer, J.A., Ramos, V.A., Ando, C.J., 1983. Andean tectonics related to geometry of subducted Nazca plate. Geol. Soc. Am. Bull. 94 (3), 341–361. https://doi.org/10.1130/0016-7606(1983)94<341:ATRTGO>2.0.CO;2.
Kay, S.M., Abbruzzi, J.M., 1996. Magmatic evidence for Neogene lithospheric evolution of the central Andean "flat-slab" between 30°S and 32°S. Tectonophysics 259 (1–3), 15–28. https://doi.org/10.1016/0040-1951(96)00032-7.
Kissling, E., Ellsworth, W., Eberhart-Phillips, D., Kradolfer, U., 1994. Initial reference models in local earthquake tomography. J. Geophys. Res. 99 (B10), 635–19,646. https://doi.org/10.1029/93JB03138.
Klein, F., 1978. Hypocenter Location Program Hypoinverse: Part I. Users Guide to Versions 1, 2, 3, and 4. Part II. Source Listings and Notes (No. 78-694). US Geological Surveyhttps://doi.org/10.3133/ofr78694.
Levina, M., Horton, B.K., Fuentes, F., Stockli, D.F., 2014. Cenozoic sedimentation and exhumation of the foreland basin system preserved in the Precordillera thrust belt (31–32 S), southern central Andes, Argentina. Tectonics 33 (9), 1659–1680. https://doi.org/10.1002/2013TC003424.
Linkimer, L., Beck, S., Zandt, G., Alvarado, P., Anderson, M., Gilbert, H., Zhang, H., 2020. Lithospheric structure of the Pampean flat slab region from double-difference tomography. J. S. Am. Earth Sci. 97, 102417. https://doi.org/10.1016/j.jsames.2019.102417.
Meigs, A.J., Nabelek, J., 2010. Crustal-scale pure shear foreland deformation of western Argentina. Geophys. Res. Lett. 37 (11). https://doi.org/10.1029/2010GL043220.
Monsalvo, G., Alvarado, P., Sáez, M., Linkimer, L., Bilbao, I., 2014. Deformación sísmica reciente de la Sierra de Pie de Palo, Provincia de San Juan. Rev. Asoc. Geol. Argent. 71 (2), 260–266.
Mooney, W., Prodehl, C., Pavlenkova, N., 2002. Seismic velocity structure of the continental lithosphere from controlled source data. Int. Geophys. Ser. 81 (A), 887–910. https://doi.org/10.1016/s0074-6142(02)80261-3.
Ortiz, D., Zambrano, J., 1981. La provincia geológica Precordillera Oriental. 13° Congreso Geológico Argentino, Neuquén, Argentina. 3, pp. 59–74.
Ottemöller, L., Voss, P., Havskov, J., 2014. Seisan Earthquake Analysis Software for Windows, SOLARIS, LINUX and MACOSX.
Pardo, M., Comte, D., Monfret, T., 2002. Seismotectonic and stress distribution in the central Chile subduction zone. J. S. Am. Earth Sci. 15 (1), 11–22. https://doi.org/10.1016/S0895-9811(02)00003-2.
Pardo, M., Monfret, T., Vera, E., Yañéz, G., Eisenberg, A., 2004. Flat-slab to steep subduction transition zone in central Chile-western Argentina: body waves tomography and state of stress. Eos (Transactions, American Geophysical Union), series 85 (47) (Fall Meeting supplement, abstract B 164).
Pavlis, G., Booker, J., 1983. Progressive multiple event location (PMEL). Bull. Seismol. Soc. Am. 73, 1753–1777.
Pérez, S., Ammirati, J., Alvarado, P., Vujovich, G., 2015. Constraining a mafic thick crust model in the Andean Precordillera of the Pampean flat slab subduction region. J. S. Am. Earth Sci. 64, 325–338. https://doi.org/10.1016/j.gr.2012.09.011.
Perucca, L., Bastías, H., 2011. Quaternary active transpression in the north of western Precordillera (San Juan and La Rioja, Argentina). Cenozoic Geology of the Central Andes of Argentina. In: Salfity, J.A., Marquillas, R.A. (Eds.), Cenozoic Geology of the Central Andes of Argentina. Instituto del Cenozoico, Universidad Nacional de Salta, Salta, Argentina, pp. 327–334.
Perucca, L.P, Vargas, N., 2014. Neotectónica de la provincia de San Juan, centro-oeste de Argentina. Boletín de la Sociedad Geológica Mexicana 66 (2) 291-204.
Pujol, J., 1988. Comments on the joint determination of hypocenters and station corrections. Bull. Seismol. Soc. Am. 78, 1179–1189.
Pujol, J., Chiu, J., Smalley, R., Regnier, M., Isacks, B., Chatelain, J., Vlasity, J., Vlasity, D., Castano, J., Puebla, N., 1991. Lateral velocity variations in the Andean foreland in Argentina determined with the JHD method. Bull. Seismol. Soc. Am. 81 (6), 2441–2457.
Ramos, V., 1999a. Las provincias geológicas del territorio argentino. Geología Argentina 29 (3), 41–96.
Ramos, V., 1999b. El segmento de subducción horizontal de los Andes Centrales Argentino-Chilenos. Acta Geol. Hisp. 32 (1), 5–16.
Ramos, V., Escayola, M., Mutti, D., Vujovich, G., 2000. Proterozoic- early Paleozoic ophiolites of the Andean basement of southern South America. In: Ophiolitic and Oceanic Crust: New Insights From Field Studies and the Ocean Drilling Program. GSA, Sp. Paper 349, pp. 331–349.
Ramos, V., Cristallini, E., Pérez, D., 2002. The Pampean flat-slab of the Central Andes. J. S. Am. Earth Sci. 15, 59–78. https://doi.org/10.1016/S0895-9811(02)00006-8.
Ramos, V.A., 1984. Patagonia, Un continente a la deriva? In: 9° Congreso Geológico Argentino. Actas, Bariloche, Río Negro, Argentina. 2, pp. 311–325.
Ramos, V.A., 1988. Late Proterozoic-early Paleozoic of South America-a collisional history. Episodes 11 (3), 168–174.
Ramos, V.A., 2004. Cuyania, an exotic block to Gondwana: review of a historical success and the present problems. Gondwana Res. 7 (4), 1009–1026. https://doi.org/10.1016/S1342-937X(05)71081-9.
Ramos, V.A., Folguera, A., 2009. Andean flat-slab subduction through time. Geol. Soc. Lond., Spec. Publ. 327 (1), 31–54. https://doi.org/10.1144/SP327.3.
Ramos, V.A., Vujovich, G.I., 2000. Descripción geológica hoja 3169–IV San Juan (Provincia de San Juan). In: Secretaria de Energía y Minería, SEGEMAR, Instituto de Geología y Recursos Minerales Boletín. 243. pp. 82.
Ramos, V.A., Jordan, T.E., Allmendinger, R.W., Mpodozis, C., Kay, S.M., Cortés, J.M., Palma, M., 1986. Paleozoic terranes of the central Argentine-Chilean Andes. Tectonics 5 (6), 855–880. https://doi.org/10.1029/TC005i006p00855.
Ramos, V.A., Dallmeyer, D., Vujovich, G.I., 1998. Ar/Ar constraints in the age of deformation of the Pie de Palo basement: implications for the docking of Precordillera and Chilenia. In: Pankhrust, R.J., Rapela, C.W. (Eds.), The Proto-Andean Margin of Gondwana. Geol. SOC., London. Spec. Pub. 142. pp. 143–158.
Ramos, V.A., Vujovich, G., Martino, R., Otamendi, J., 2010. Pampia: a large cratonic block missing in the Rodinia supercontinent. J. Geodyn. 50 (3–4), 243–255. https://doi.org/10.1016/j.jog.2010.01.019.
Rapela, C.W., 2000. The Sierras Pampeanas of Argentina: Paleozoic building of the southern proto-Andes. In: Tectonic Evolution of South America, pp. 381–387.
Regnier, M., Chatelain, J.L., Smalley, R., Chiu, J.M., Isacks, B.L., Araujo, M., 1992. Seismotectonics of Sierra Pie de Palo, a basement block uplift in the Andean foreland of Argentina. Bull. Seismol. Soc. Am. 82 (6), 2549–2571.
Regnier, M., Chiu, J., Smalley, R., Isacks, B., Araujo, M., 1994. Crustal thickness variation in the Andean foreland, Argentina, from converted waves. Bull. Seismol. Soc. Am. 84 (4), 1097–1111.
Reta, M.C., 1992. High Resolution View of the Wadati-Benioff Zone and Determination of the Moho Depth in San Juan, Argentina. [M.Sc. thesis]. Memphis State University (98p).
Richardson, T.J., Gilbert, H.J., Anderson, M.L., Ridgway, K.D., 2012. Seismicity within the actively deforming Eastern Sierras Pampeanas, Arg. Geophys. J. Int. 188, 408–420. https://doi.org/10.1111/j.1365-246X.2011.05283.x.
Richter, C., 1935. An instrumental earthquake magnitude scale. Bull. Seismol. Soc. Am. 25, 1–32.
Rivas, C., Ortiz, G., Alvarado, P., Podesta, M., Martin, A., 2019. Modern crustal seismicity in the northern Andean Precordillera, Argentina. Tectonophysics 762, 144–158. https://doi.org/10.1016/j.tecto.2019.04.019.
Rolleri, E.O., 1969. Rasgos tectónicos generales del valle de Matagusanos y de la zona entre San Juan y Jocolí provincia de San Juan, República Argentina. Rev. Asoc. Geol. Argent. 24, 40–412.
Ruskin, B.G., Jordan, T.E., 2007. Climate change across continental sequence boundaries: paleopedology and lithofacies of Iglesia Basin, Northwestern Argentina. Journal Sedimentary Research 77, 661–679. https://doi.org/10.2110/jsr.2007.069.
Sánchez, G., Recio, R., Marcuzzi, O., Moreno, M., Araujo, M., Navarro, C., Suárez, C., Havskov, J., Ottemöller, L., 2013. The Argentinean national network of seismic and strong-motion stations. Seismol. Res. Lett. 84 (5), 729–736. https://doi.org/10.1785/0220120045.
Siame, L., Sebrier, M., Bellier, O., Bourles, D., Castano, J., Araujo, M., Yiou, F., Raisbeck, G., 1996. Segmentation and horizontal slip-rate estimation of the El Tigre Fault Zone, San Juan Province (Argentina) from spot images analysis. In: 38° International Symposium of Andean Geodynamics. St Malo, France, Extended Abstracts, pp. 239–242.
Smalley, R., Isacks, B., 1987. A high-resolution local network study of the Nazca Plate

Wadati-Benioff Zone under western Argentina. J. Geophys. Res. Solid Earth 92 (B13), 13903–13912. https://doi.org/10.1029/JB092iB13p13903.
Smalley, R., Isacks, B., 1990. Seismotectonics of thin- and thick-skinned deformation in the Andean foreland from local network data: evidence for a seismogenic lower crust. J. Geophys. Res. Solid Earth 95 (B8), 12487–12498. https://doi.org/10.1029/JB095iB08p12487.
Smalley, R., Pujól, J., Regnier, M., Chui, J., Chatelain, J., Isacks, B., Araujo, M., Puebla, N., 1993. Basement seismicity the Andean Precordillera thin-skinned thrust belt and implications for crustal and litospheric behavior. Tectonics 12 (1), 63–76. https://doi.org/10.1029/92TC01108.
Snoke, J.A., 2003. FOCMEC: FOCal MEChanism Determinations. Virginia Tech, Blacksburg, VA. USA, pp. 1629–1630. https://doi.org/10.1016/S0074-6142(03)80291-7.
Spalletti, L.A., Cingolani, C.A., Varela, R., Cuerda, A.J., 1989. Sediment gravity flow deposits of an Ordovician Deep-sea fan system (western Precordillera, Argentina). Sediment. Geol. b1, 287–301. https://doi.org/10.1016/0037-0738(89)90063-8.
Stacey, F.D., Davis, P.M., 2008. Physics of the Earth, 4th edition. Cambridge University Press pp 513.
Steinberger, B., 2000. Plumes in a convecting mantle: Models and observations for individual hotspots. J. Geophys. Res. 105 (B5), 11127–11152. https://doi.org/10.1029/1999JB900398.
Stuessy, T.F., Foland, K.A., Sutter, J.F., Sanders, R.W., Silva, M., 1984. Botanical and geological significance of potassium-argon dates from the Juan Fernández Islands. Science 225 (4657), 49–51. https://doi.org/10.1126/science.225.4657.49.
Thomas, W.A., Astini, R.A., 1996. The Argentine Precordillera: a traveler from the Ouachita embayment of North American Laurentia. Science 273, 752–757. https://doi.org/10.1126/science.273.5276.752.
Thomas, W.A., Astini, R.A., 2003. Ordovician accretion of the Argentine Precordillera terrane to Gondwana: a review. J. S. Am. Earth Sci. 16 (1), 67–79. https://doi.org/10.1016/S0895-9811(03)00019-1.
Val, P., Venerdini, A., Ouimet, W., Alvarado, P., Hoke, G., 2018. Tectonic control of erosion in the southern Central Andes. Earth Planet. Sci. Lett. 482, 160–170. https://doi.org/10.1016/j.epsl.2017.11.004.
Venerdini, A., Sánchez, G., Alvarado, P., Bilbao, I., Ammirati, J., 2016. Nuevas determinaciones de velocidades de ondas P y ondas S para la corteza sísmica del terreno Cuyania en el retroarco andino. Revista Mexicana de Ciencias Geológicas 33 (1), 59–71.
Vigny, C., Rudloff, A., Ruegg, J.C., Madariaga, R., Campos, J., Alvarez, M., 2009. Upper plate deformation measured by GPS in the Coquimbo gap, Chile. Phys. Earth Planet. Inter. 175 (1–2), 86–95. https://doi.org/10.1016/j.pepi.2008.02.013.
Volponi, F., 1968. Los terremotos de Mendoza del 21 de Octubre de 1968 y la estrnctura de la corteza terrestre, in Acta Cuyana de Ingenietla. San JuanInstituto Sismológico Zonda, Facultad de Ingeniería, Universidad Nacional de Cuyo, Argentina, pp. 95–110.
Von Gosen, W., 1992. Structural evolution of the Argentine Precordillera: the Río San Juan section. J. Struct. Geol. 14 (6), 643–667. https://doi.org/10.1016/0191-8141(92)90124-F.
Von Huene, R., Corvalán, J., Flueh, E., Hinz, K., Korstgard, J., Ranero, C., Weinrebe, W., 1997. Tectonic control of the subducting Juan Fernández Ridge on the Andean margin near Valparaiso, Chile. Tectonics 16 (3), 474–488. https://doi.org/10.1029/96TC03703.
Vujovich, G.I., van Staal, C.R., Davis, W., 2004. Age constraints on the tectonic evolution and provenance of the Pie de Palo Complex, Cuyania composite terrane, and the Famatinian Orogeny in the Sierra de Pie de Palo, San Juan, Argentina. Gondwana Res. 7 (4), 1041–1056. https://doi.org/10.1016/S1342-937X(05)71083-2.
Wessel, P., Smith, H.W., 1991. Free software helps map and display data. EOS Trans. Am. Geophys. Union 72 (41), 441–446. https://doi.org/10.1029/90EO00319.
Yáñez, G., Cembrano, J., Pardo, M., Ranero, C., Selles, D., 2002. The Challenger-Juan Fernández-Maipo major tectonic transition of the Nazca-Andean subduction system at 33–34°S: geodynamic evidence and implications. J. S. Am. Earth Sci. 15, 23–38. https://doi.org/10.1016/S0895-9811(02)00004-4.
Zapata, T.R., Allmendinger, R.W., 1996. Thrust front zone of the Precordillera, Argentina: a thick skinned triangle zone. Bull. Am. Assoc. Pet. Geol. 80 (3), 350–381.